ADDIS ABABA UNIVERSITY

SCHOOL OF GRADUATE STUDIES

CHARACTERIZATION OF MAJOR SUBSURFACE STRUCTURES IN ADA'A PLAIN USING INTERGATED GEOPHYSICAL SURVEY

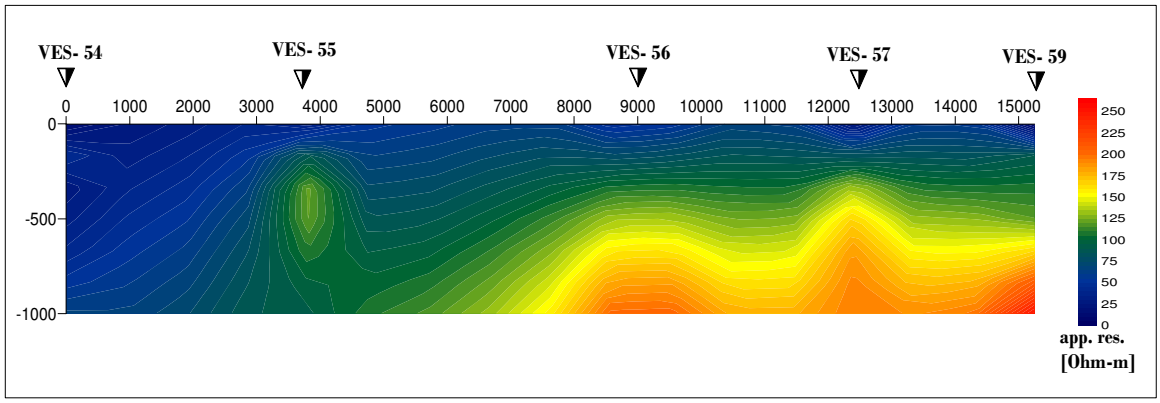

ASSEFA GETANEH

FEBRUARY 2007

CHARACTERIZATION OF MAJOR SUBSURFACE STRUCTURES IN ADA'A PLAIN USING INTERGATED GEOPHYSICAL SURVEY

A THESIS PRESENTED TO THE SCHOOL OF GRADUATE STUDIES OF
ADDIS ABABA UNIVERSITY
IN PARTIAL FULFILLMENT OF THE REQUIREMENT FOR THE DEGREE
MASTER OF SCIENCE IN EXPLORATION GEOPHYSICS

BY

ASSEFA GETANEH

ADDIS ABABA
2007

ADDIS ABABA UNIVERSITY

School of Graduate Studies

CHARACTERIZATION OF MAJOR SUBSURFACE STRUCTURES IN ADA'A PLAIN USING INTERGATED GEOPHYSICAL SURVEY

By
Assefa Getaneh

Department of Earth Sciences

Approved by the Examining board:

Name	**Signature**
Dr.Tigistu Haile Examiner (Internal)	_____
Ato Moges Tigabe Examiner (External)	_____
Dr.Shemelis Fisseha Advisor	_____
Dr.Balemewal Atsenafu Department Chairman	_____

DEDICATION

This work is thoroughly dedicated to W/o Tarik Addis. She is mom indeed.

ACKNOWLEDGEMENTS

It is with great pleasure that I particularly acknowledge my Advisor Dr. Shimeles Fisseha for his company during field operation, comments on substantial parts of the manuscript and continuous encouragement to complete the project.

Dr. Tigistu Haile, my favorite teacher, deserves acknowledgement for providing me reading materials and an orientation on the proton precision magneto-meter.

I am also very thankful to Water works design and Supervision (WWDSE) for providing the raw and processed data used in this project.

The Geological Survey of Ethiopia is Acknowledged for giving me corrected and processed data relevant to this work.

Thanks are also due to Ato Engida Zemedkun for sharing ideas about the problem, my friend Gashaw Sisay who was on my side through out the time of writing and editing the manuscript.

My final thanks must be to my wife W/o Aberu and son Yohannes, my sisters W/o Menalu and her family, W/o Etagegn and her family, Eskedar, Beamlak, my brothers Addisu and his family and Dereje who have contributed a lot, one way or another, to the completion of this work.

Table of Contents

ii

List of Figures

ABSTRACT

This manuscript presents the results of geophysical data analysis from Ada'a plane with a primary objective of characterizing major subsurface structures and their connection to the subsurface hydraulic system. Towards this end, verifying a barrier, inferred through preliminary interpretations and conceptualizations of the ground water system in the plane by Water Works Design and Supervision Enterprise (WWDSE), was the primary task of this work.

Ada'a ground water is located in the southern Awash Basin, Oromiya Regional State, between geographical coordinates of $38^0$50'E - $39^0$15'E and $8^0$30'N - $8^0$45'N.

The geophysical data set employed in this project includes: the potential field methods namely Gravity and Magnetics and are used to investigate major subsurface structures. The other method found adequate for this study is the electrical resistivity method as it is used to evaluate ground water potentials.

Regional and residual Bougeur anomaly contour maps revealed large scale regional subsurface structures that align along the rift and small scale, local subsurface structures showing different orientation. The residual feature with a discordant structural alignment shows spatial correlation with the expected subsurface barrier. The total field magnetic contour map also confirms this indication and gave further evidence for the existence of such anomalous feature in the area of interest.

A depth-slice stack map of apparent resistivity of fifty VES data also manifested a subsurface feature that coincide to the anomaly revealed by the residual gravity map. Deep, low apparent resistivity responses, which can safely be interpreted as water saturated, aquifer zones, are separated by a high resistivity, elongated feature. This feature could represent an impermeable dry rock units related to domes and cones of intermediate magma that can possibly impede the ground water movement.

Inversion of 2D electrical resistivity imaging data gave a clear subsurface picture and depicted the geo-electric substratum, which is a resistive dry bottom, to rise above the expected water table at the speculated region. Though it falls short to cover the lateral extension of the inferred barrier, it presented strong evidence that supports findings from the other methods. A 1D apparent resistivity pseudo-section along VESs 54,55,56,58 and 59 reflect the geologic reality as they traverse across a high resistive formation where the barrier is expected lying and complement the results of the 2D analysis.

CHAPTER ONE

1. Introduction

1.1 General

Some studies are being undertaken, by Water Works Design and Supervision Enterprise, (WWDSE), on consultant basis, on Ada'a Plain for the Evaluation of Groundwater Potential and Design of pressurized irrigation development. The project is designed and sustained by Ministry of Water Resource, as a client.

Geophysical investigations, as a major component of the multi-disciplinary study, were carried out to supplement the ongoing work by giving some additional subsurface geological and hydro geological information.

This manuscript presents the geophysical component of this integrated study as part of the thesis project for postgraduate program in exploration geophysics. It has four chapters. The first chapter is introduction and presents general insight on the location, geology and hydro-geological set up of the project area. Moreover, the main objectives and scope of the study are also presented in the first chapter. Chapter two discusses the basic principles of the geophysical methods with emphasis on DC resistivity and Magnetics. Chapter three presents the data processing and interpretation procedure, used in this work. Chapter four contains discussions of the main results and interpretations. Finally, conclusions and recommendations are given in chapter five of the studies.

1.2. The Study area

1.2.1 Location, Topography and Accessibility

The study area, Ada'a plain is located in the upper part of Awash River Basin. It is specifically situated in Central Ethiopia, in Oromia Regional State, and bounded approximately, between geographic coordinates of $38^0$50'E - $39^0$15'E and $8^0$30'N - $8^0$45'N. The Ada'a plain ground water basin is found along the Addis Ababa - Djibouti high way, from 35 to 70 km of distances and topographically varies between 1600 and 1900m above the mean sea level.

The area is bordered by the Yerer Mountain and Kesem River basin, in the north, and koka reservoir in the south. The total area of Ada'a plain is estimated to be more than 1500$km^{2.}$

The mean annual rainfall of the study area is about 902mm, and, the mean monthly temperature varies from 16 to 22^0c.

The study area is covered by an extensive lacustrine deposit over the flat area, with isolated hills and mountains like mount-Ziquala. A number of small lakes scattered within small area, at and near by Debre Zeit town. Dukem and Mojo are the other main towns situated at the western and eastern extremes of the study area, respectively.

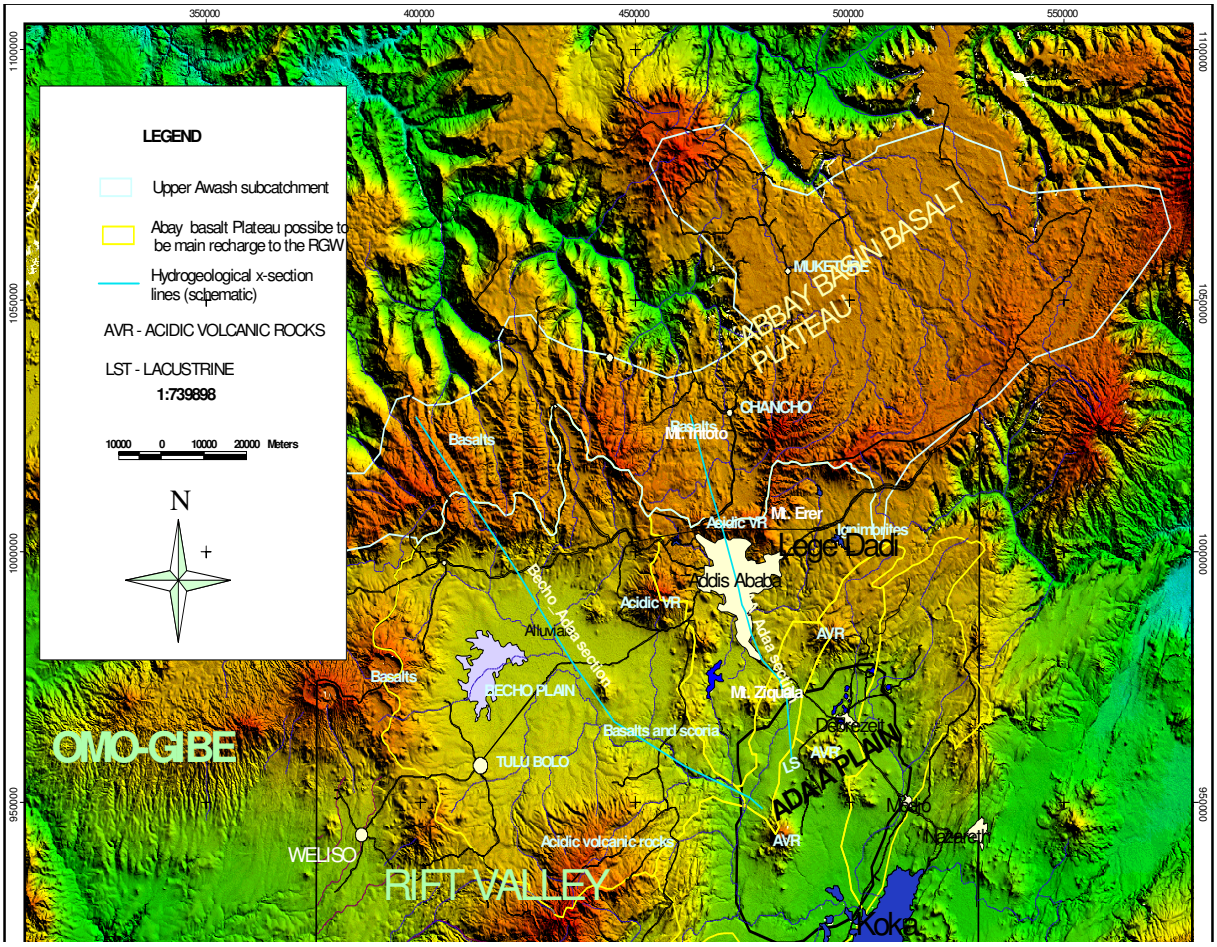

Figure 1.1 Digital topographic model of central Ethiopia, showing the location of Ada'a plain.

During dry seasons, the study area is accessible by dusty roads. Rainy seasons, however, make accessibility to the study area difficult. A location map of the study area is shown in figure 1.1.

1.2.2. Regional Geology

The regional geology of the area is characterized by a series of formation and events from early Tertiary to Quaternary era. The grand Afro-

Arabian swell was formed in upper Eocene. Following uplift of horn of Africa, immense quantities of lavas, the Trap series, extruded from fissures and eruption centers (Mohr, 1961).

The trap series lavas, which are mostly basaltic in composition (with some acidic flows in the upper parts), cover large areas of Mesozoic sediments and in some places; they rest directly on the Basement complex. Such uplifts, together with the extrusion of thick and extensive Trappean lava, account for the formation of the present highland region of Ethiopia.

In the upper Pliocene to recent, a succession of pantelleritic Rhyololites, Trachytes and Ignimbrites with subordinate intermediate and basic rocks, were erupted chiefly at the rift margins and along the seismically active Wonji fault. This trachyte-pantelleritic ignimbrite covered most of the southern Ethiopian plateau and filled the Main Ethiopian Rift. Its thickness ranges from about 300m to 500m, probably even greater on the rift floor (Mohr 1968, Baker et al. 1972).

1.2.3. Tectonics

The Tertiary - Quaternary system, known as the East African system, is one of the largest structural features of the earth crust. It is widely believed that diverging lithospheric plates have formed them, since early Tertiary times. It extends from Mozambique to Syria. The east African system is most typically developed in the section as the main Ethiopian Rift (Mohr, 1964), which extends from lake Chamo, in the south, to Afar in the north. The main Ethiopian Rift is characterized by NE-SW, and ENE-WSW trending normal faults. According to previous studies in and around the project area, lineaments (faults) are predominantly trending NE-SW with dip towards NW and SE respectively.

1.2.4. Geology of Debre-Zeyit

The area around Debre-Zeyt, (where Ada'a plain occupies a larger proportion) is mainly covered by volcanic and sedimentary rocks. The sedimentary rocks consist of alluvial cover and lacustrine sequences. Volcanic activity in the area resulted in central composite volcanoes and monogenic apparatea as domes, spatter cones and maars. Ignimbrites, consisting of several units, appear as wide sub-horizontal covers, while basaltic lavas are generally tabular.

The detailed (1:100,000) geological map of Debre Zeyt (F. Mazzarini, 1999) recognize ten volcanic units that were grouped into four volcanic complexes. These were defined on the basis of field data and morpho-structural features, further they define three main structural sectors; the western rift margin, the main rift floor and an intra-rift depression. Since upper Miocene, the Debre Zeyt area was the site of the interaction between the Main Ethiopian Rift and an E-W traverse structure (Yerer-Tullu Wellel Volcanic Lineament,YTVL) that produced the smoothing of the morphological expression of the rift margin and the onset of a secondary rift axis associated with the most recent volcanic activity (F. Mazzarini, 1999).

A simplified geological map of Debre zeyt modified from (Abebe, et al., 1999) is shown on figure 1.2

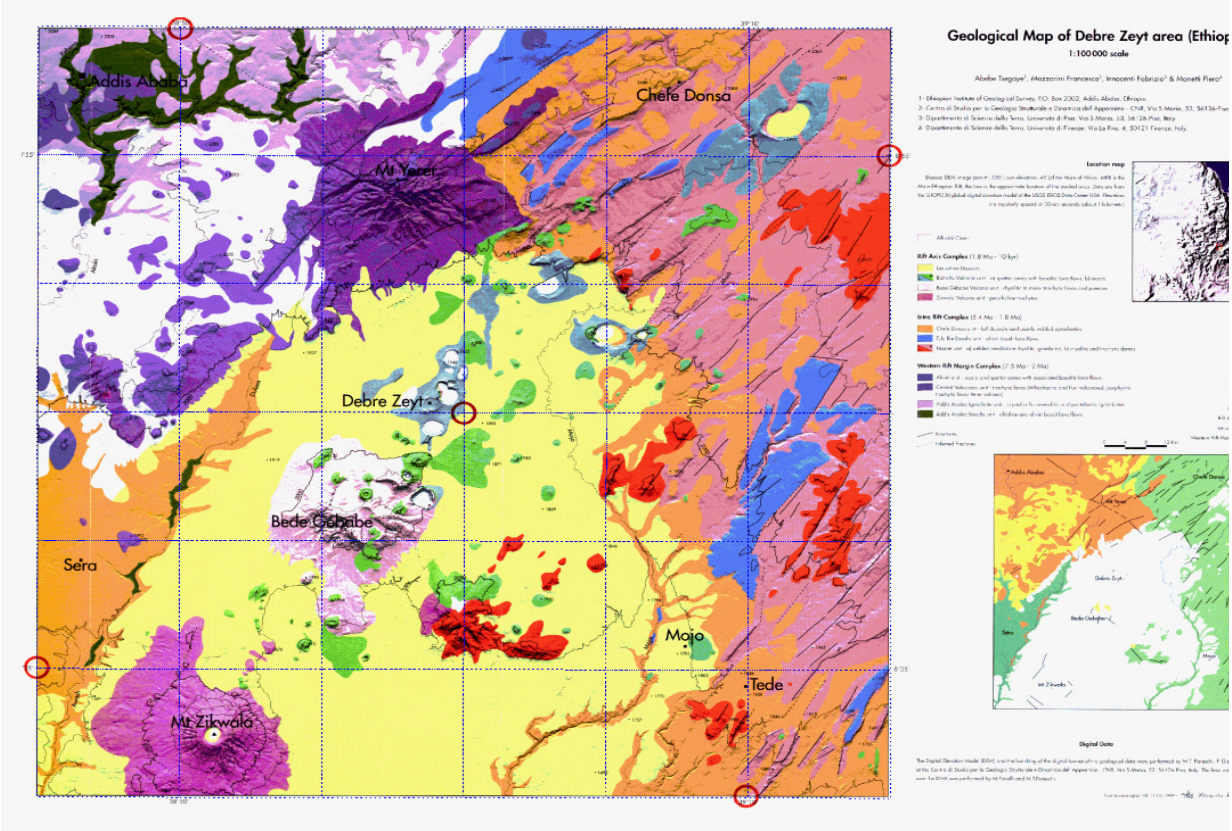

Figure 1.2 Geological map of Ada'a plain and Debre zeyit area *(modified from Abebe, et al., 1999)*

1.2.5. Hydrogeology of Ada'a Plain

The lacustrine sediments show a lot of differences in their permeability, those showing the highest are ones consisting of volcanic sands, water lain volcanic sands (such as those around Debre Zeit and Metehara). On the other hand, fine-grained sediments with interbedding of massive tuffs and fine ash are also known. (Tesfaye Cherinet, 1986).

The aquifers of Ada'a plain are lacustrine sediments, scoria, scoraceous basalt and vasicular basalts (volcanic aquifers). The thickness of lacustrine sediments can reach up to 100m, underlain by scoraceous basalt.

The volcanic aquifers have primary porosities like vesicles, and secondary porosities like faults, fractures and fissures produced as a result of tectonic activities and weathering. Generally, in the volcanic ground, water circulation and occurrence (storage) is associated with those porosities, while in the alluvial and Lacustrine aquifers, it is in the interstitial spaces between the sediments.

In the rift floor the geological complexity has created a highly segmented ground water distribution although the regional groundwater flow is from the escarpment into the valley and north -eastwards to Lake Abbe. (HLCROW, 1989).

Review of previous studies, available data (Tibebe, 2006; and inception report of Water Works and Design Enterprise) show that: Ada'a plain can be categorized, based on the depth to the ground water, into two zones.

The first zone (Zone I) is north - east of Bede Gebaba volcanoes. In this zone the groundwater depth is relatively shallow (30-40m) and all Debre Zeit lakes are concentrated in this zone.

The second zone (Zone II) is found south - west of Bede Gebaba. The surface elevation of this zone is lower than the first. The groundwater depth is relatively deep reaching down to 100m and, at some places, even deeper. The main reason for the difference in depth of groundwater level between these two zones could be the barrier condition of the acidic volcanic rocks of Bede Gebaba.

The most important features governing the groundwater flow and storage in volcanic rocks are, vertical permeability due to primary and secondary fractures or horizontal permeability due to horizon

containing opening due to the lava flow and gas expansion during solidification or due to occurrence of impervious horizons and dykes.

In the volcanic terrain, it is possible to find potential water bearing horizons intercalated with relatively impervious units. In such aquifers groundwater occurs under confined conditions. Inter-bedding of massive units with fractured and porous media also gives rise to multi - layer aquifer system. (Tibebe, 2006)

1.3. Hydrogeological boundaries

Geological boundaries define the volume of an aquifer and hydrogeological boundaries, specially the water table, define the volume of water stored within it. Commonly encountered geological boundaries are stratification of aquifers and of aquifers against aquicludes, the termination of aquifers by faults, unconformities and igneous intrusions (dykes, sills, etc…).

Not every geological boundary necessarily functions as a hydrogeological boundary. There must be a noticeable difference in either the storage characters of the ground, or in the chemistry of the groundwater on either side of the boundary. Hydrogeological boundaries are therefore usually revealed by a change either in water levels, or in the gradient of water levels, or in water quality. The causes of the discontinuity, marked by an abrupt drop of water level on either side of the barrier is, the barrier (the bed-rock-ridge) is virtually impermeable and impede the flow of groundwater.

1.4 Statement of the problem and main Objectives

1.4.1 Statement of the problem

Multi-disciplinary studies have been going on at Ada'a Plain for the evaluation of groundwater potential and design of pressurized irrigation development by the Ethiopian Ministry of Water Resources. Water Works Design and Supervision Enterprise is undertaking the work on consultancy basis.

The consultant has made preliminary interpretation and conceptualization of the groundwater system of the plain. Accordingly, a longitudinal profile of the Ada'a Plain, showing both the topography and potentio-metric surface, reveals that the regional hydraulic gradient seams to be affected by some geologic features. One such possibility is regional scale structure(s), acting as a hydraulic barrier that impedes the movement of the groundwater. The water level contour also shows that the depth to the water table is reversed, appearing deeper at topographically low areas. Moreover, linear geologic structures, anticipated from aerial photo and Land-Sat imagery interpretations, are thought to have some connection with the regional hydro-geological regime (Figure-1.1). This called for the use of integrated geophysical investigation to verify the inferred groundwater barrier and its possible connection to surface geologic structures.

The first effort was made by (Tibebe, 2006), as part of a research project for M.SC dissertation, by employing limited geophysical data then available.

Using few resistivity soundings and a single profile magnetics data, Tibebe (2006) concluded that the subsurface groundwater barrier, at the position anticipated on previous geological repots, was not detected or mapped. Latter on however, the Enterprise's technical team came up

with a different orientation for the barrier than previously reported and carried out further geophysical investigations, including two-dimensional resistivity imaging. The second phase geophysical campaign resulted in adequate coverage of the area of interest by electrical methods.

In the present research work, it was proposed to process and analyze all geophysical data availed by the enterprise, to date, and was undertaken accordingly. Additional geophysical data was also collected and integrated to the existing data-base. Moreover, a reduced regional gravity data (obtained from the Ethiopian geological survey data base) has also been incorporated in order to come up with a broader picture of the major subsurface geological structures for a better understanding of the hydro-geological setting of the Ada'a plain.

The existing data availed by the enterprise for this work includes:

1. Fifty Vertical Electrical Sounding (VES) data
2. 2D resistivity imaging data along a 17 km long profile and,
3. A digital topographic model, few Bore-hole log data and other relevant information.

1.4.2 OBJECTIVES AND SCOPE OF THE STUDY

The specific objectives of the work are:

1) Analyzing the 2D resistivity imaging data of the Dukem profile using available modeling and inversion programs. This is primarily aimed at out-lining the anticipated subsurface groundwater barrier,

2) Mapping the regional configuration of electrical resistivity structure of the project area, at different depth levels, using VES data, in order to demarcate the geo-electrical zoning,

3) Compiling regional gravity and semi-regional magnetic maps of the study area for the purpose of delineating subsurface geologic structures and study their possible connection with the anticipated barrier, and finally;

4) As a post-graduate geophysics student, imparting a practical knowledge in the state of the art of interpretation methods, thereby, showing the merit of integrated geophysical investigation for evaluating the groundwater resources and its role in establishment of regional models.

CHAPTER TWO

2. THEORETICAL AND MATHEMATICAL BASIS OF ELECTRICAL RESISTIVITY AND MAGNETIC METHODS

2.1. General

Geophysical investigations of the interior of the earth involve taking measurements at or near the earth's surface that are influenced by the internal distribution of physical properties. Analysis of the geophysical data reveals the distributions of physical properties at depth that reflect the subsurface geology.

Depending on the source of signals, geophysical methods fall into two major groups.

- ***Passive methods*** are those that detect variations within the natural fields associated with the Earth, such as the gravitational and magnetic fields.

- ***Active methods*** are in contrast to the passive methods, such as used in exploration seismology, in which artificially generated signals are transmitted into the ground, which then modifies those signals in ways that are characteristics of the materials through which they travel. Appropriate detectors whose output can be displayed and ultimately interpreted measure the altered signals.

Though, almost all geophysical survey methods have wide scope of utilizations, there is always one physical property for which a particular method is exceptionally sensitive and as such determines its specific range of application . And few, if any, geophysical methods provide a unique solution to a particular geophysical situation. It is possible to obtain a very large number of geophysical solutions to some problems, some of which may be

geophysically nonsensical. However, a number of geophysical methods may be applied simultaneously (integrated geophysical exploration) in solving certain geophysical problems, and such approach, greatly reduces the problem of ambiguity, which is the inherent drawback in the interpretations of results from one method, by complementing the information gap from the additional methods. Moreover; it is of paramount importance that geophysical data are interpreted within a physically constrained or geological framework.

A descriptive treatment of the more important aspects concerning on developing fundamental understanding of electrical resistivity and magnetic methods and the physical principles on which they are based are discussed briefly in this section.

2.2 Electrical resistivity method

2.2.1 Basic concept and scope

Electrical resistivity methods were developed in the early 1900s but have become very much more widely used since the 1970s, due primarily to the availability of computers to process and analyze the data. These techniques are used extensively in the search for suitable ground water sources and also to monitor types of ground water pollution; in engineering surveys to locate sub-surface cavities, faults and fissures, etc; and in archeology for mapping out the areal extent of remnants of buried foundations of ancient buildings, amongst many other applications. Electrical resistivity methods are also used extensively in down hole logging (Reynolds, 1997).

Resistivity is a fundamental electrical property of rocks closely related to their lithologic compositions. In the electrical resistivity method a direct or a low frequency alternating current is introduced into the ground by means of two electrodes (current electrodes) connected to the terminals of a portable source of electromotive force (emf). The resulting potential distribution on the ground, mapped by means of two non-polarizable electrodes (potential

electrodes) is capable of yielding information about the distribution of electrical resistivity below the surface. The method is efficient when good electrical contact with the ground is secured. Thus, it is not effective in regions with non-conducting surface formations like dry desert rocks, frozen ground, etc.(Dobrin, 1988 and Parasnis, 1986).

2.2.2 Electric conduction in continuous medium

The electric current in a short thin, linear conductor of uniform cross-section, is given by Ohm's law:

$$I = -\frac{\Delta V}{R} \qquad \text{..... (1)}$$

Where 'I' is the current in ampere (A), ΔV is the potential difference in volts (v) between the ends of the conductor and R is the resistance of the conductor in ohms (Ω). The minus sign expresses the fact that the current flow is from high to low potential (opposite to the increase of potential gradient).
Since resistance is directly proportional to the length l in meters (m) of the conductor and inversely proportional to the cross-sectional area A in square meters (m^2),

$$R = \rho \frac{\lambda}{A} \qquad \text{..... (2)}$$

Where, the constant of proportionality ρ is the resistivity in ohmmeters (Ω-m) of the material of the conductor.

The distinction between resistance and resistivity is that resistance is an opposition that a particular path of an electric current offers to the flow the

current where as resistivity is one of the physical properties of a conductor that determines its electric resistance.
Substituting equation (2) in equation (1) for R and rearranging gives

$$\frac{I}{A} = -\frac{1}{\rho}\frac{\Delta V}{\lambda} \quad \text{..... (3)}$$

The left-hand side of equation (3) is the current density j (current per unit area of cross-section in $A/m^{2)}$, while $-\Delta V/\ \ell$ on the right hand side is the electric field E in v/m in the direction of the current density vector.
Hence,

$$J = \frac{E}{\rho} \text{ ..... (4)}$$

Since resistivity ρ is the inverse of conductivity σ in siemens per meter (s/m) or mho,
And equation can alternatively be written as

$$J = \sigma E \text{ ..... (5)}$$

When the length ℓ in equation (3) tends to zero and if one considers the linear conductor as a homogeneous and isotropic continuous medium, then either of equation (4) or (5) expresses Ohm's law for such a medium. The electrical resistivity method is based on Ohm's law, which in more generalized form, states that the electric field strength at a point, in an electrically isotropic material, is directly proportional to the current density passing that point.

2.2.3. Current flow in a homogeneous, isotropic Earth

An electrically isotropic medium is the one for which the resistivity ρ, is a scalar function of the point of observation and the current density **J,** is in the same direction as the electric field vector, **E.**

In an anisotropic medium, **J** has a directive property and, in general, is not in the direction of E. This calls for some modification in Ohm's law as:

$$J_x = \sigma_{xx}E_x + \sigma_{xy}E_y + \sigma_{xz}E_z$$

$$J_y = \sigma_{yx}E_x + \sigma_{yy}E_y + \sigma_{yz}E_z$$

$$J_z = \sigma_{zx}E_x + \sigma_{zy}E_y + \sigma_{zz}E_z \quad \text{.....(6)}$$

2.
2.
3.

1 Point current source

The resistivity method consists of measuring potential P_1 when current is applied at a point source A. The return current electrode can be placed at a very great distance and assume material of uniform resistivity ρ. Because air has infinite resistivity, no current flows upward. Thus, current flows radially outward through the earth equally in all directions so as to define a hemispherical surface (Fig.2.1). Since current distribution is equal everywhere on this surface, which is at a distance r from the current electrod A, the potential also is equal. These surfaces are known as equipotential surfaces.

By defining a very thin shell of thickness dr and developing eqn. (3), one can define the potential difference across the shell to be

$$dV = -I\rho\frac{d\lambda}{A} = -I\rho\frac{dr}{2\pi r^2} \quad \text{.....} \quad (7)$$

The potential at a point far away by convention is arbitrarily defined to be equal to zero. The most direct way to determine V is to integrate

eqn. (6) over its distance r_1 to the current electrode to infinity (Van Nostrand and Cook, 1966), or

$$V = \int_{r_1}^{\infty} dv = -\frac{I\rho}{2\pi}\int_{r_1}^{\infty} dr / r^2 = \frac{I\rho}{2\pi r^2} \quad \text{..... (8)}$$

Equation (8) determines the potential at p_1. This equation is the fundamental equation in electrical resistivity prospecting discussions and it is possible to use it to develop more practical relationships as will be seen in the following sections.

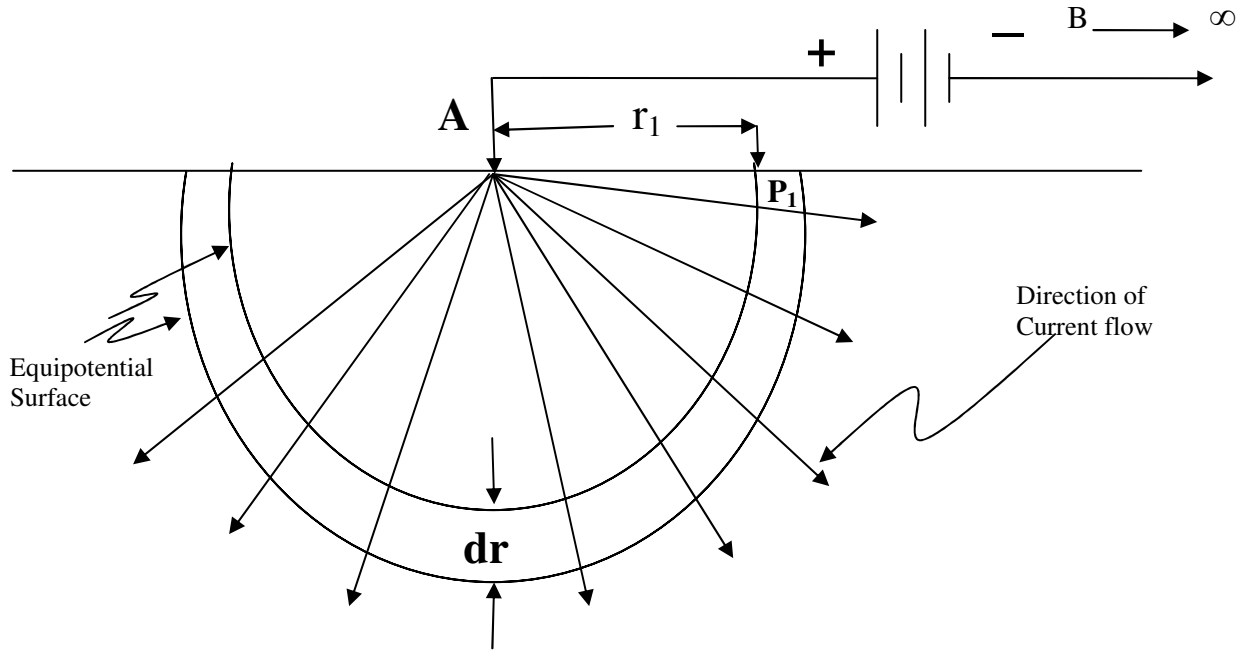

Figure 2.1 Diagram illustrating symbols and configurations used to determine the potential at P_1 for a single point source of current A. The two equipotential surfaces shown are separated by the distance dr, where, $d\ell = dr$ and $A = 2\pi r^2$

The information, which can be obtained from eqn. (8) by assuming a constant resistivity and current, is that it enables to map the potential at any point in section view of Fig. (2.1). If adequate number of points were plotted one can draw lines through those points possessing the same potential. This defines the equipotential surfaces. Therefore, the direction of current flow can be determined, because current must be perpendicular to these equipotential surfaces.

2.2.3.2 Two current electrodes

In a homogenous isotropic earth with two current electrodes the current must flow from the positive current electrode (the source) to the negative current electrode (the sink).

The derivation, for the case when the current electrodes and the potential point lie in the same plane as shown in figure2.1, is that the potential at point P_1 is determined by using equation (8).

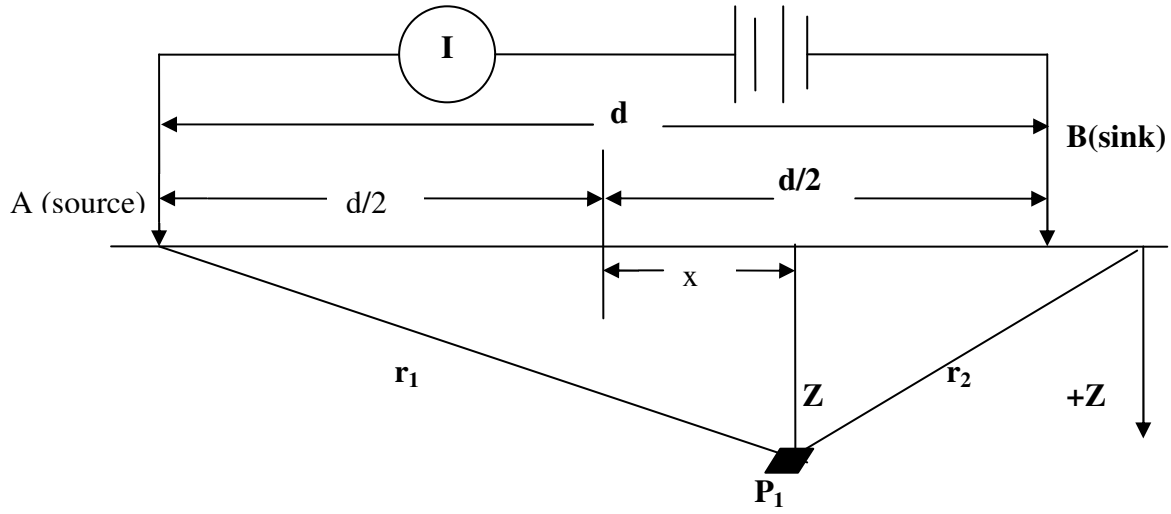

Figure 2.2 Diagram illustrating symbols and configurations used to determine potential at P_1 for a current source A and sink B.

The effect of the source at A(+) and the sink at B(-) are both considered, and therefore,

$$V_{p1} = \frac{I\rho}{2\pi r_1} + \left[\frac{-I\rho}{2\pi r_2}\right] = \frac{I\rho}{2\pi}\left[\frac{1}{r_1} - \frac{1}{r_2}\right] \quad \text{..... (9)}$$

Expressing r_1 and r_2 of x-z coordinate system shown in Fig. (2.2), eqn. (9) can be written as:

$$V_{p1} = -\frac{I\rho}{2\pi}\left\{\frac{1}{\left[\left[\frac{d}{2} + X\right]^2 + Z^2\right]^{\frac{1}{2}}} - \frac{1}{\left[\left[\frac{d}{2} - X\right]^2 + Z^2\right]^{\frac{1}{2}}}\right\} \quad \text{..... (10)}$$

This equation is used for a computer-contouring package of the distribution of equi-potential surfaces.

The current flow lines are perpendicular to the equipotential lines, but the manner in which current is distributed is not known. The mathematical analysis to determine the current distribution is fairly complicated but results in a simple equation that provides current distribution as a fraction of the total current (Van Nostrand and Cook, 1966). Along a vertical plane midway between two current electrodes Fig. (2.2), the fraction of the total current I_f penetrating to depth z for an electrode separation dr given by (Burger, 1992)

$$I_f = 2\pi \tan^{-1}\left[\frac{2z}{d}\right] \text{..... (11)}$$

Current distribution for various electrode separations can be investigated using eqn. (11). Therefore, for a homogeneous isotropic subsurface, the

greater the electrode separation the greater the depth to which a given percentage of current penetrates.

2.2.3.3. Two potential electrodes

In electrical resistivity surveying, the potential difference between two points is measured. Fig (3) illustrates two potential electrodes M and N that are located on the surface as are the current electrodes. Using eqn.(9), derived to determine the potential at a point due to a source and sink, the potential difference can be obtained by determining the potential at one point electrode M and subtracting from it the potential at N.

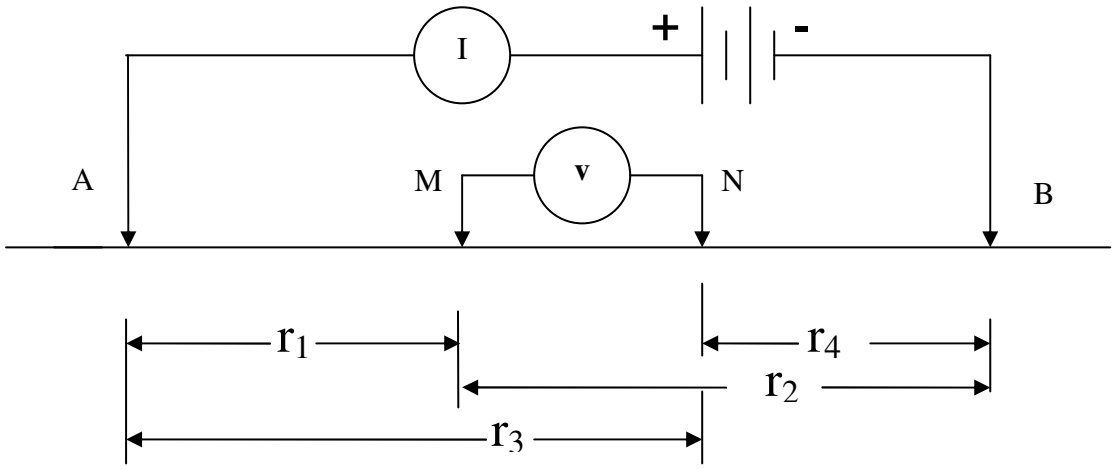

Fig.(2.3) Diagram used to determine potential difference at two potential electrodes M and N.

Using eqn. (9)

$$V_{p1} = \left[\frac{I\rho}{2\pi r_1} - \frac{I\rho}{2\pi r_2} \right] \qquad \text{..... (12)}$$

and

$$V_{p2} = \left[\frac{I\rho}{2\pi r_3} - \frac{I\rho}{2\pi r_4} \right] \quad \text{..... (13)}$$

Therefore, the potential difference ΔV equals

$$\Delta V = V_{p_1} - V_{p_2} = \left[\frac{I\rho}{2\pi r_1} - \frac{I\rho}{2\pi r_2} \right] - \left[\frac{I\rho}{2\pi r_3} - \frac{I\rho}{2\pi r_4} \right] \text{..... (14)}$$

Or

$$\Delta V = \frac{I\rho}{2\pi} \left[\frac{1}{r_1} - \frac{1}{r_2} - \frac{1}{r3} + \frac{1}{r_4} \right] \text{..... (15)}$$

In electrical resistivity method, a known current is entered into the ground, potential difference is measured, and resistivity can be determined. Because resistivity is unknown quantity, one can solve for the resistivity ρ from equation (15) and obtain

$$\rho = 2\pi \frac{\Delta V}{I} \left[\frac{1}{r_1} - \frac{1}{r_2} - \frac{1}{r_3} + \frac{1}{r_4} \right]^{-1} \text{..... (16)}$$

2.2.3.4. Apparent resistivity

Before discussing the various electrode spreads, it is necessary to consider what is actually measured by any array of current and potential electrodes. From eqn. (15)

$$\rho = K \frac{\Delta V}{I} \text{..... (17)}$$

Where $$K = 2\pi\left[\frac{1}{r_1} - \frac{1}{r_2} - \frac{1}{r_3} + \frac{1}{r_4}\right]^{-1} \quad \text{..... (18)}$$

K is the geometric factor which depends on the electrode disposition.
By measuring ΔV and I and knowing the electrode configuration, one obtains the resistivity ρ. Over homogeneous isotropic ground the resistivity will be constant for any current electrode arrangement. For non-homogeneous ground, however, as the electrode spacing is varied or the spacing remains fixed while the whole array is moved then the ratio will in general change. This results in a different value of ρ for each measurement. The magnitude is intimately related to the arrangement of electrodes. This measured quantity is known as *apparent resistivity* ρ_a. Although it is diagnostic, to some extent, to the actual resistivity of a zone in the vicinity of the electrode array, the apparent resistivity is definitely not an average value and only in the case of homogeneous ground it is equal to the actual resistivity (Telford et al. 1990).

2.2.4 Common electrode configurations

In actual practice a number of conventional surface configurations are used for the current and potential electrodes. In many arrangements, both sets of electrodes are laid out along a line. The current electrodes are generally placed on the outside of the potential electrodes (symmetrical). The most widely used configurations will be described in the paragraphs that follow. For convenience V will denote the measured potential while the potential difference is denoted by ΔV.

2.2.4.1 Wenner array

One common electrode arrangement for resistivity measurement is the Wenner array (configuration) illustrated in Fig. (2.4a). Here each potential electrode is separated from the adjacent current electrode by a distance 'a', which is one-third the separation of the current electrodes. For this

arrangement, setting $r_1 = r_4 = a$ and $r_2 = r_3 = 2a$ in eqn.(16), the apparent resistivity becomes

$$\rho_a = 2\pi a \frac{\Delta V}{I} \quad \text{...} (19)$$

2.2.4.2 Schlumberger array

In the Schlumberger configuration, the operator expands the electrode spacing by increasing the distance between current electrodes, typically on a logarithmic scale, during the course of measurements. The potential-electrode spacing is assumed to be infinitesimal, and the observed values of potential can be adjusted accordingly. The Schlumberger electrode arrangement is illustrated in Fig.(2.4b)

The apparent resistivity at the center of a Schlumberger array, $r_1 = r_4 = (s - a/2)$ and $r_2 = r_3 = (s + a/2)$ in eqn.(16), yields

$$\rho_a = \pi \frac{\left(s^2 - a^2/4\right)}{a} \frac{\Delta V}{I} \quad \text{.....................................} (20)$$

Where,'s' is half of the current electrode separation (i.e. AB/2).

The Wenner arrangement is a special case of the Schlumberger array, in which s = 3a/2

2.2.4.3 Dipole-dipole array

The dipole-dipole array, some times called the double dipole, has the two current electrodes (A and B) and the two potential electrodes (M and N) well separated and exterior to each other. The dipole-dipole array is illustrated in Fig.(2.4c). For symmetrical dipole-dipole array the dipoles align and the separations a and b are equal and one considers the measure point as the mid point between B and M which is the center of symmetry of the configuration. The distance between B and M (the dipole separation) is

usually an integer multiple, n, of the distance between the current or potential electrode pair. Initially, n (the dipole separation factor) is set to 1. Then it is increased to 2,3, and so on until a maximum value of between 4 and 6. When n is increased, the potential measured between M and N decreases rapidly. For this reason, it is not advisable to use a value of n greater than 6. Using larger value of n could result in rather noisy data. In some surveys, the distance "a" between the current and potential electrode pairs is doubled or tripled to increase the signal strength. Thus both the dipole separation factor (n) and the spacing between the current electrode pair (a) has to be recorded. The depth of investigation increases with the spacing between the centers of the respective pairs : L = (n+1)a. By setting $r_1=r_4=(n+1)a$, $r_2=na$ and $r_3=(n+2a)$ in equation (16) the apparent resistivity determined by this array is given by

$$\rho_a = n(n+1)(n+2)\pi a \frac{\Delta V}{I} \quad \text{..... (21)}$$

2.2.4.4 Pole-dipole array

The electrode configuration for the pole-dipole array is illustrated in Fig.(2.4d). Electrode A remains fixed and is located far enough away from the array for the measurement to depend only on the electric field from electrode B. The separation between B and M is an integral multiple, n, of the separation between the potential electrodes (n=1, 2, 3, etc.). The pole-dipole array is an asymmetrical array, and over symmetrical structures the apparent resistivity anomalies in the pseudosections are also asymmetrical. In some situations, the asymmetry in the measured apparent resistivity values could influence the model obtained after inversion. One method to eliminate the effect of this asymmetry is to repeat the measurements with the electrodes arranged in the reverse manner. (Fig.2.4e).

Setting $r_1=r_4=\infty$ and $r_2=na$ and $r_3=(n+1)a$ in eqn. (16) yields

$$\rho_a = 2\pi an(n+1)\frac{\Delta V}{I} \quad \text{.....(22)}$$

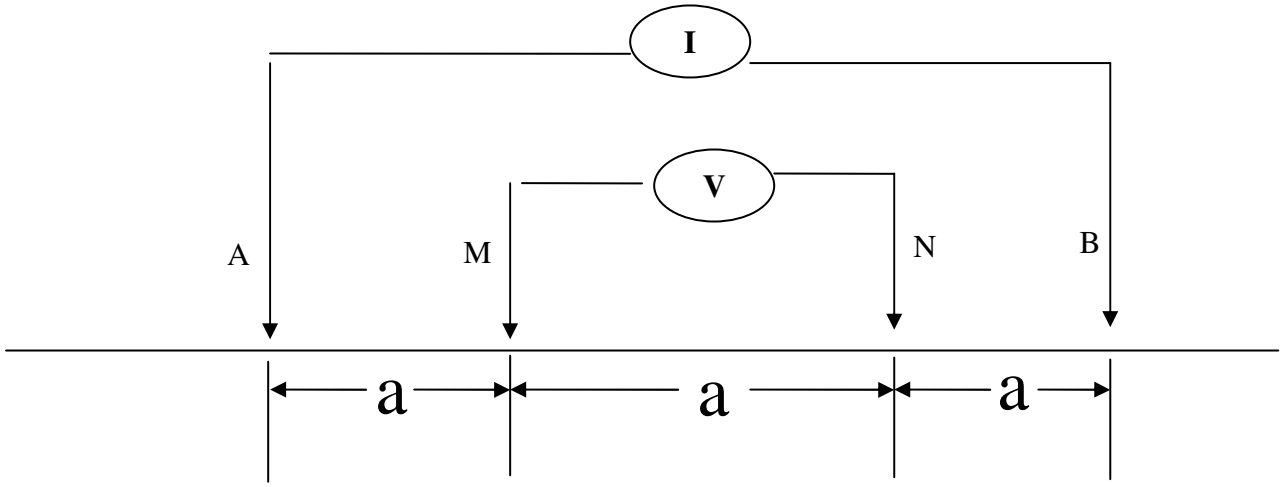

(a)

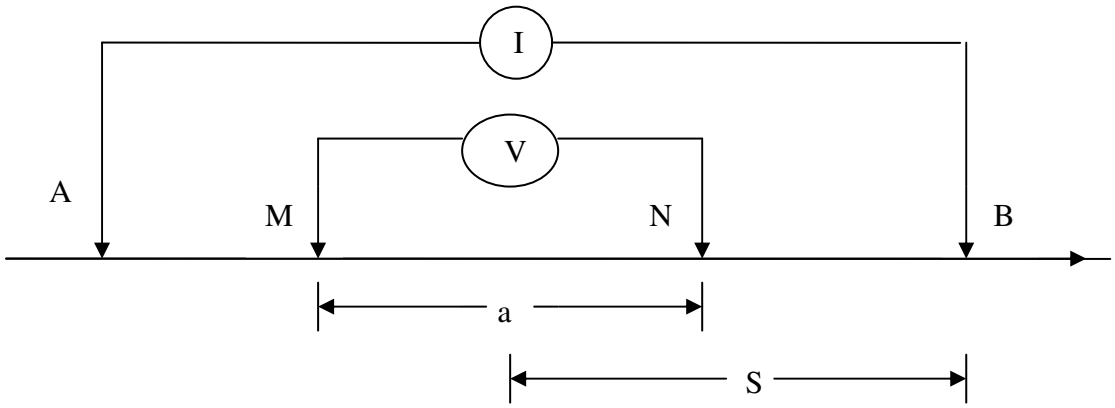

(b)

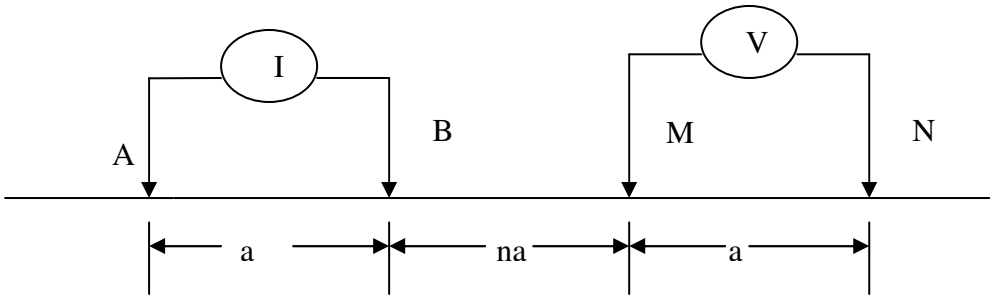

(c)

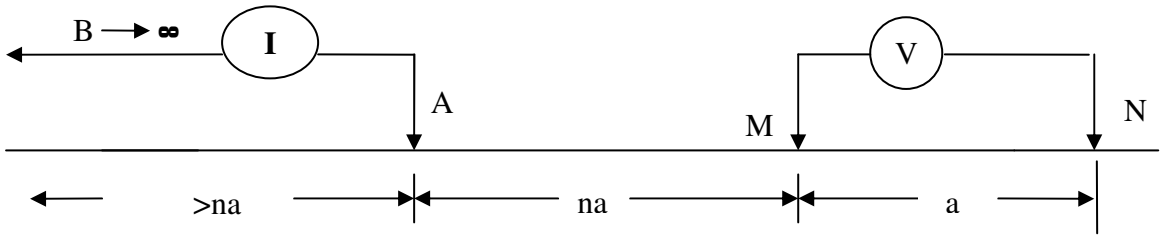

(d)

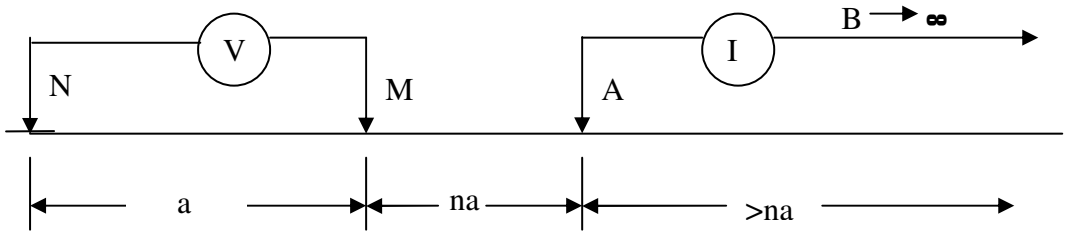

(e)

Fig*ure* 2.4, Collinear electrode configurations in common use: (a) Wenner (b) Schlumberger (c) dipole-dipole(axial) (d) pole-dipole(forward) (e) pole-dipole(reverse)

2.2.5 Comparison of electrode arrangements

Some of the advantages and disadvantages of Wenner, Schlumberger, Dipole-dipole and pole-dipole electrode arrangements as explained by (Zohdy et al., 1974) are presented in the sub-sections that follow.

Wenner array

Advantages:

- The apparent resistivity is simple to calculate
- Can be operated with less power since potential electrodes (MN) are spaced (AB/3) apart, where AB is the separation between the current electrodes.
- Convenient for profiling (horizontal investigation) as for each station, previously defined electrode positions can be used.

Disadvantages:

- To expand the electrode spread, all four electrodes must be moved to a new position, hence more manpower is required and more time is ”consumed” for each reading.
- Because all four electrodes have a big effect on the data, the result is more sensitive to local in homogeneities, as potential electrodes are moved after each measurement in a sounding.
- Interpretive aids are less advanced than for the Schlumberger system
- More sensitive to cross coupling effects
- Depth of investigation is less than in other arrays.

Schlumberger array

Advantages:

- Less manpower required because of only the current electrodes need to be moved at each and every sounding measurement. If at all, the potential electrodes need only be moved occasionally.
- Less sensitive to cross-coupling (potential leads shorter)
- Less sensitive to lateral inhomogeneties because potential electrodes generally remain fixed. Also if they are moved, lateral effects can be distinguished from layering effect.
- better depth of investigation than for the Wenner array
- better resolution between layers with different resistivities
- Interpretive aids are generally more developed than for the Wenner array (standard curves, auxiliary graphs, etc.)

Disadvantages:

- More power required as potential electrodes are closer together (small ΔV’s). Alternatively more sensitive equipment is required.

Dipole-dipole array

Advantages:

- Short AB and MN lines can be used to explore great depths, that is, depth investigation and resolution is better than that of schlumberger configuration.
- It needs short cables
- Fewer problems of current leakage and inductive coupling because of shorter cables

Disdvantages:

- Large power required for depth penetration (to produce measurable potential)
- data not so straight forward to interpret
- interpretation procedures and programs are not abundantly available

Pole-dipole array

Advantages

- Only three electrodes are moved and this saves time in field operation
- The current signal decreases less quickly with depth than that of the dipole-dipole array and this enables deeper investigation less noisy.

Disadvantages

- The pole-dipole array is an asymmetrical array, and over symmetrical
- Structures, the apparent resistivity anomalies in the pseudosections are also asymmetrical. In some situations, the asymmetry in the measured
- Apparent resistivity values could influence the model obtained after inversion.

2.2.6 Resistivity field survey procedures

The two basic procedures to be used in resistivity work, depending on whether one is interested in resistivity variation with depth or lateral extent, respectively, are Vertical Electrical Sounding (VES) and Lateral Profiling.2D (two dimensional) electrical imaging may also be used when both lateral and vertical variations of electrical resistivity of the subsurface is thought.

2.2.6.1 Vertical electrical sounding

Since the fraction of total current that flows at depth varies with the current electrode separation as described in section 2.2.3.2., the field procedure is to use a fixed center with expanded spread. Although the pole-dipole array is not suited to this technique, any if the three configurations mentioned above may be used.

The Schlumberger array is best used for VES, because the potential electrodes remain fixed while the current electrode spacing is expanded symmetrical about the center of the spread. For large values of AB/2 it may be necessary to increase MN/2 also in order to maintain a measurable potential. The Schlumberger array is more convenient for VES than the Wenner expanding array because only two electrodes need move at a time. In addition, the effect of shallow resistivity variations is constant with fixed potential electrodes.

The presence of horizontally or gently dipping beds of different resistivities is best detected by the expanding spread. Hence the method is useful in determining depth of overburden, depth, structure, and resistivity of flat-lying sedimentary beds and possibly of the basement also if it is not too deep.

It is frequently necessary to carry out this expanding procedure at several locations in an area, even when the main interest may be in lateral exploration, to establish the proper electrode spacing for the lateral search (Telford et. al., 1990).

2.2.6.2 Lateral profiling

Resistivity profiling is particularly useful in mineral exploration, where the detection of isolated bodies of anomalous resistivity is required. It is also used in studying steeply dipping contacts (faults, dykes, shear zones and steeply dipping veins), or for the lateral change in the resistivity of a particular horizon. In resistivity profiling, the spacing between the electrodes is held constant and the array is moved as a whole along the traverse line. Apparent resistivity is plotted against the mid point of the potential electrodes for symmetrical arrays (Telford et al., 1990; Keller and Frischknecht, 1966).
A given distance between current and potential electrodes corresponds to a set of data related to a nearly constant depth of investigation and thus, to a layer of earth of a given thickness. The dimensions of the configuration will then be chosen as a function of the depth of the problem in question.

2.2.6.3 2D Electrical Imaging

2D (two dimensional) electrical imaging may also be used when both lateral and vertical variations of electrical resistivity of the subsurface is thought. The survey is usually carried out with systems where the electrodes are arranged along a line.

To achieve a deeper depth of investigation the electrode separation in the Wenner array, the separation between the current electrodes in the Schlumberger array, the dipole separation in the dipole-dipole array, or the separation between the current electrode and the adjacent potential electrode is increased by a factor of "n" where n = 1,2,3,...,6.

2.3 Magnetic Method

The magnetic method of prospecting is the oldest geophysical method and is applied in various degrees for mineral, oil, gas, coal and groundwater explorations as well as for geotechnical and archaeological site investigations

(Dobrin, 1988). The method is especially effective to map structural features like faults, fractures and/or contact zones which often serve as potential hosts for a variety of minerals and/or conduits for movement of ground water. In oil, gas and coal exploration the method is mainly used as a reconnaissance tool to assist in outlining and determining the thickness of the sedimentary basin and areal extent of the potential area. Commonly in the larger exploration investigations, both magnetic and gravity methods are used to complement each other. Used together prior to seismic survey, they can provide more information about the subsurface, particularly the basement rocks, than either technique on its own.

2.3.1 Basic Magnetic Theory

The Earth's Magnetic Field: The knowledge of the earth's magnetic properties and conditions of the earth as a whole is necessary as magnetic measurements are made within the magnetic field of the earth. The earth's magnetic field at a given place and time is believed to have:

- An external origin - which is due to the solar wind, a constant stream of ionized particles emitted from the sun. It makes 0.5% of the field and is the cause for the diurnal variation of the total field;
- An internal origin-which is due to magnetic field of the dipole field generated at the outer core.
- Magnetism of rocks associated with geological structures.

Magnetic field variations produced due to this field is the chief interest in magnetic prospecting and it designates the anomaly part.
The earth's total field intensity is not perfectly symmetric about the geographical poles due to local variations in the distribution of magnetic minerals within the earth's crust. The field variation with time is also observed due to the effect of solar wind that reaches in the range of 50-100nT and magnetic storms in the order of 50 nT as they distort the magnetosphere or the external magnetic field of the earth. The earth's internal or main field

also changes slowly over many years through what is termed as the secular variation. The inclination, intensity and even the location of the poles varies slowly (Breiner, 1973). To isolate the anomaly part, that is, the field due to local magnetized bodies within the earth's crust, the main field and the diurnal parts must be removed as the geomagnetic observation is necessarily affected by the sum of all the three parts.

Magnetic field strength: The force *F* between two poles with strength P_0 and P separated by a distance r is expressed as

$$F = \frac{\mu_o P_o P}{4\pi\mu_r r^2} \qquad \text{.....(23)}$$

When F is in Newtons, P in ampere-meters and r in meters, μ_0 the permeability of free space, is given in Newton per square ampere (N A^2), μ is the relative permeability of the medium separating the poles, and is dimension less. The magnetic field strength at a point is defined as the force per unit of pole strength, which would be exerted on a small pole of strength P_0 if placed at that point. Thus, the field strength *H* due to a pole of strength P at a dista:

$$\mathbf{H} = \frac{\mathbf{F}}{p_o} \quad \textbf{or} \quad H = \frac{\mu_o p}{4\pi\mu_r r^2}$$

$$H = \frac{1}{P_o} \quad 4\pi\mu_r r^2 \qquad \text{.....(24)}$$

where **H** is in Ampere per Meter.

Magnetic Induction: A magnetic body when placed in an external field H has its internal poles more or less lined up by the field **H** to produce a field of its own **H'**, which increases the total field within the body. This extra field is related to the intensity of magnetization **I** as (Parasnis, 1975).

$$\mathbf{H'} = 4\pi\mathbf{I} \qquad \text{.....(25)}$$

Where, the induced intensity of magnetization **I**, i.e., the magnetic moment per unit volume, acquired by the body due to a magnetizing force **H** is given by

$$\mathbf{I} = k\mathbf{H} \qquad \text{.....(26)}$$

Where, k is magnetic susceptibility of the body.

The intensity of magnetization is an import property of rocks which has great significance in magnetic prospecting.

The magnetic effect of a homogeneously magnetized body depends on the grain size of the magnetic minerals, their distribution within the rock mass and also the direction of magnetization.

The magnetic induction B is defined as the total field with in the body, i.e.,

$$\boldsymbol{B} = \boldsymbol{H} + \boldsymbol{H'} \quad \text{.....(27)}$$

Substituting for **H'** from eqns. (25) and (26)

$$\boldsymbol{B} = (1 + 4\pi k)\,\boldsymbol{H} \quad \text{.....(28)}$$

where $(1 + 4\pi k) = \mu_r$ is the relative magnetic permeability, **H** is an intrinsic magnetic strength and B represents the induced magnetic field plus an intrinsic magnetic field.

In SI system of units H is measured in Ampere per meter, whereas B is in Weber per square meter. In the cgs system, where one unit of electric current (absolute-ampere) is 10 ordinary Ampere, i.e., 1 ab Ampere = 10 Ampere, magnetic induction B is measured in Gauss (G) and H - in Oersted. Because these units are large, a nanotesla (nT) or gammas (γ) is used to measure the magnetic field strength in magnetic prospecting (Parasnis, 1975 and Telford 1976).

$1\gamma = 10^{-5}$ G = 1 nT.

Earth's Magnetic Field Elements: The direction and magnitude of the geomagnetic field at any point on the earth's surface are represented by a vector parallel to the direction of the field pointing in the direction of force on a positive pole and having a length proportional to the strength of the field at that point. This vector is referred to a set of mutually perpendicular axes directed astronomically north and east and vertically downward (fig.2.5).

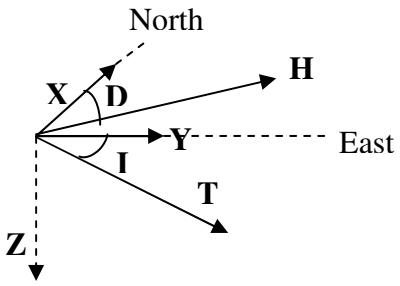

Figure 2.5 Earth's magnetic field elements

The total field (**T**), the vertical (**Z**) and the horizontal (**H**) components of the field, the inclination (**I**) and declination (**D**) are important components involved in magnetic prospecting (Breiner 1973). The magnetic elements as illustrated in Fig.1 are related as follows:

$$\left.\begin{array}{l} H = T\cos I \quad X = H\cos D \quad X^2 + Y^2 = H^2 \\ Z = T\,\mathrm{Sin}\, I = H\tan I: \quad Y = H\,\mathrm{Sin}\, D \quad H^2 + Z^2 = T^2 \end{array}\right\} \quad \ldots\ldots\ldots\ldots\ldots(29)$$

Where, X and Y are the horizontal components of vector H.

These quantities can also be derived from magnetic potential V. In spherical coordinates, the Vertical (Z) and horizontal (H) components of the total field (T) are defined as

$$Z = \frac{\partial V}{\partial r} \quad ; \quad H = \frac{1}{r}\frac{\partial V}{\partial \theta} \quad \ldots\ldots\ldots\ldots\ldots\ldots\ldots\ldots(30)$$

where **T = Z + H**

For example, assuming a dipole of potential V = ($\mu_o/4\pi$) M Cos 0/r^2 located at the center of the earth, the horizontal and vertical components of the total magnetic field at an external point of distance r from the center is derived from the potential as follows (fig2.6):

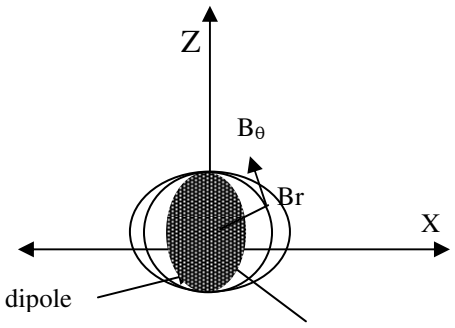

Figure 2.6. Schematic representation of the earth's magnetic field

$$B_\theta = H = \frac{1}{r}\frac{\partial V}{\partial \theta} = \frac{\mu_o M \sin\theta}{4\pi r^3} \qquad \text{.....(31)}$$

$$B_r = Z = \frac{\partial V}{\partial r} = \frac{2\mu_o M \sin\theta}{4\pi r^3} \qquad \text{.....(32)}$$

where M = 2 l p (l the dipole length) is the magnetic moment, and θ is the magnetic latitude.

Substituting for μ_0 (= 4π x 10^{-7} N/A^2), M (= 7.9 x 10^{22} Am^2), and r (= 6.4 x 10^6 m, for the radius of the earth) in eqns. (9) and (10), the horizontal and vertical components of the total magnetic field are nearly 0 and 60,000 nT, respectively, along the north pole (θ = 0^0) and the south pole (θ = 180^0). Thus, at polar regions the total field has only vertical component. On the other hand, at the equator where θ = 90o, the magnitudes are 30,000 nT and 0 for the horizontal and vertical components, respectively. Here the total field has a horizontal component which is only half the magnitude at polar regions.

Magnetic Properties of Rocks: The magnetism of practically all rocks is controlled by their content of magnetic minerals like magnetite, hematite, pyrrhotite, ilmenite and some others. Magnetite is by far the most magnetic and the most common. Although the variation of susceptibilities is considerable, it is possible to generalize that magnetite, pyrrhotite, ilmenite and some chromite and manganese-bearing ores have large susceptibilities; while pyrite, zinc, and galena are characterized by lower susceptibility values.

Minerals such as graphite and quartz have negative susceptibility values. Rocks like basalts, diabases, skarns and some granulites as well as pegmatities are much more magnetic than sedimentary rocks like limestones, sandstones and slates (Breiner, 1973 and Nettleton, 1976).

2.3.2 Magnetic anomaly

A magnetic anomaly represents a local disturbance in the earth's magnetic field which arises from a local change in magnetization or a magnetization contrast. The form of the magnetic anomaly from a given body depends on factors such as: the geometry of the body, the direction of the earth's field at the location of the body, the direction of polarization of the rocks forming the body, the orientation of the body with respect to the direction of the earth's magnetic field, the orientation of the line of observation with respect to the axis of the body, etc.(Nettleton,1976). Magnetic anomalies in the earth's field are caused by two different kinds of magnetism - the induced ($\mathbf{I_i}$) and the remnant ($\mathbf{I_r}$) magnetizations. Thus, total magnetization ($\mathbf{I}$) is a vector sum of the induced and remnant magnetizations, i.e.,

$$\mathbf{I = I_i + I_r} \quad \text{..... (33)}$$

I_1 depends on the susceptibility of the body, whereas I_r on the geologic history of the rocks.

Practically, the sources of magnetic anomalies ($\triangle T$) are the existence of ferromagnetic minerals in the crust of the earth. The contrasting proportion of these ferromagnetic minerals makes the anomaly defined as

$$\triangle T = T_{obs} - T_o - T_{sw} \quad \text{.....(34)}$$

where T_{obs} - is the total magnetic field as measured by the survey magnetometer, T_o the magnetic field due to dipole, determined from the IGRF (the International Geomagnetic Reference Field) and T_{sw} is the magnetic field due to solar wind determined from magnetogram or a base station magnetometer.

The magnitude of the magnetic anomaly $\triangle T$ (the component of the anomalous field in the direction of undisturbed total field), can also be expressed interms of its components. i.e.,

$\triangle T = \triangle H \cos I \cos\alpha + \triangle Z \sin I$ .....(35)

where $\triangle H$ and $\triangle Z$ are the horizontal and vertical components of the change in total field due to the local disturbance; I is the inclination, and α is the profile azimuth or angle between the profile and horizontal. This relation is used in modeling magnetic data for determining the parameters of the anomalous body such as depth, shape, size and dip (Breiner, 1973).

Eqn. (35) can be used to calculate the magnetic anomaly due to simple geologic structures like a dipole and a monopole at any magnetic latitude. For example, for a dipole located at the north pole (where I = 90°) (fig. 2.7a) it yields the following signature (assuming α to be zero):

$$\Delta T = \Delta Z = \frac{M(2Z^2 - X^2)}{(X^2 + Z^2)^{\frac{5}{2}}} \quad \text{.....(36)}$$

Similarly, at the equatorial region, where I = 0^0, it yields.

$$\Delta T = \Delta H = \frac{M(2X^2 - Z^2)}{(X^2 + Z^2)^{\frac{5}{2}}} \quad \text{.....(37)}$$

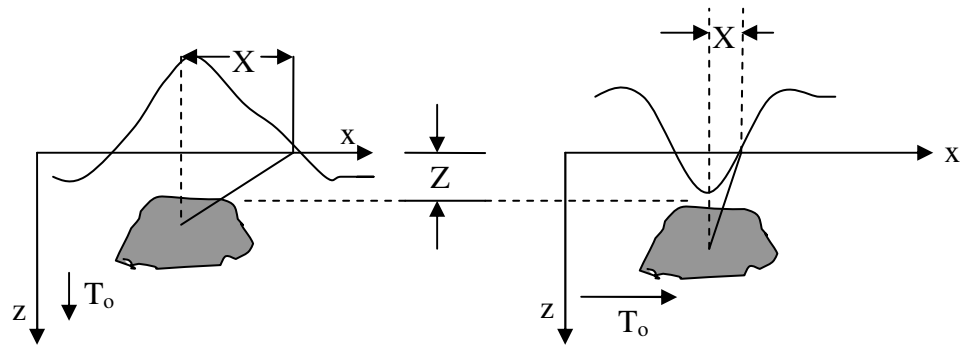

(a) (b)

Figure 2.7. Magnetic anomaly due to dipole a) at north pole and b) at the equator

The maximum amplitude of the magnetic anomaly over the earth's surface is a function of the depth and contrast in the mass of magnetic minerals and, to

a less extent, on the configuration of the source (Breiner, 1973). The basic expression for estimating the maximum amplitude of any anomaly is given by

$$\Delta T = \frac{M}{r^n} \qquad \text{.....(38)}$$

where, △T is the anomaly magnitude, M the magnetic moment, r the distance (depth) to the source, and 'n' a measure of the rate of decay of the field with distance, or fall-off rate (n=3 for a dipole, n = 2 for a monopole, etc.)(Breiner, 1973).

2.4 GRAVITY METHODS

2.4.1 Gravity and Gravimetry

Gravimetry is a method of measuring and modeling the gravity field of the earth (Torge, 1989). It is the measurement of gravity intensity, which is the magnitude of gravitational acceleration on or at the vicinity of the earth and other celestial bodies. The method of gravity survey in geophysics involves measurement, reduction, mapping and interpretation of gravity data (Dobrin, 1988).

2.4.2 Fundamental principle of gravity

The basis of the gravity survey method is Newton's law of gravitation, which states that the attraction force between two points masses mi and m^ whose dimensions are small with respect to the distance r between them, is given by:

$$F = \frac{-Gm_1m_2}{r^2} \qquad \text{.....(39)}$$

Where 'r' is the distance between the masses, 'G' is the gravitational constant which is equal to 6.67 x 10-11 m3/kg s2 and 'F' is the mutual force of attraction between m1 and m2.

Since force is the product of mass and acceleration; the acceleration of m2 is given by:

$$F = m_2 a = \frac{G m_1 m_2}{r^2} \quad \text{……..(40)}$$

As a typical example, consider a mass m on the surface of the earth:

$$F = mg = \frac{G M_e m}{r2} \quad \text{……(41)}$$

$$g = \frac{G M_e}{r^2} \quad \text{.....(42)}$$

'g' is known as the gravity field or gravity field intensity or simply gravity. The unit of 'g', practically in gravity survey, is the Gal.

2.4.3 REDUCTION OF GRAVIMETRIC DATA

Introduction

To produce the necessary information for the preparation of the final Bouguer gravity map, the following essential data must be determined at each observation point: relative gravity difference from one or more references or base stations, relative elevation for making the elevation correction and relative position for making latitude corrections and for mapping the final results. After the instruments determine the value of gravity, the following corrections are made: Free air correction, Bouguer correction, Terrain (topographic) correction, Latitude correction and Drift correction.

I. Latitude Corrections: - If the earth were a homogenous non-rotating sphere with the same vertical gradient everywhere, apart from local near surface density variations due to geological structures, and if it were a perfectly smooth surface, then clearly all gravity variations over the surface would be caused by geological structure. But this is not so. Because of the flattening, the poles are nearer to the center of mass than the equator, so the gravity increases with increasing in latitude. The variation of gravity with latitude over the surface of an ellipsoid earth can be expressed using the

theoretical gravity formula (TGRS1967). The latitude correction δgL is obtained by differentiating the theoretical gravity formula and is added to g as one moves towards the equator, i.e.

$$\frac{\delta g_{L}}{\delta s} = \frac{1}{r}\frac{\delta g_{\phi}}{\delta \phi} = 0.811 \sin 2\phi mGal \quad \text{.....(43)}$$

Where r = 6371km is the radius of the earth, and △s = rδΦ = N-S horizontal distance, and Φ is the latitude angle (Telford, 1990).

II. Free Air Correction: -The free air correction is based on the fact that the attraction of the earth as a whole can be considered to be the same as if its mass were concentrated at its center. The free air correction takes into account the fact that each station is a different distance from the earth's center than the datum plane. If the elevation of a gravity meter is changed, its distance from the center of the earth changes by the same amount. The inverse-square law enables one to predict how much the acceleration of gravity will change as a result. Most stations are above sea level; the force of gravity becomes progressively less as the altitude becomes greater. So it is necessary to correct for changes in elevation between stations to reduce observations to a datum surface (Telford, 1990). The correction is obtained by differentiating equation (42) for a spherical earth.

The gravity at a point located at a height 'h' above the geoid is (Telford, 1990)

$$g_h = \frac{GM}{(r+h)^2} = \frac{GM}{\left\{r^2\left(1+\frac{h}{r}\right)^2\right\}} = \left\{\frac{GM}{r^2}\right\}\left(1+\frac{h}{r}\right)^{-2} \quad \text{.....(44)}$$

Applying the Binomial expansion for the term (l+h/R)2 and ignoring higher order terms and taking only the first two terms gives

$$g_h = \left(\frac{GM}{r^2}\right)\left(1-\frac{2h}{r}\right) \quad \text{.....(45)}$$

The free air correction is therefore given by

$$\delta g_{FA} = g - g_h = \frac{2gh}{r} = 0.3086 mGal/m \quad \text{.....(46)}$$

Note that the free air correction is added to the gravity reading when the station is above the geoid and subtracted when below it.

III. Bouguer Correction:- Rock masses between the station and sea-level increase the value of gravity; the amount being proportional to the altitude of the station and the density of the rocks between the station and sea-level. The Bouguer correction accounts for the attraction of the excess material between the station and the datum plane, which was ignored in free air correction. If the station were centrally located on a plateau of large horizontal extent and uniform thickness and density of gravity readings would be increased by the effect of this slab between the station and the datum plane. It is the correction for the attraction as approximated by considering the material as an infinite horizontal slab. The gravity attraction for a point on the surface of a slab obtained by calculating the effect of an infinite disk is given by

$$\delta g_B = 2G\rho h \quad \text{...(47)}$$

where h is the height of the gravity station above the geoid and G is the gravitational constant and ρ is the density. For mean crustal density (ρ = 2.67 gm/cm3) and h in meters, the Bouguer correction reduces to

$$\delta g_B = 0.1119 h \text{mGal/m} \quad \text{...(48)}$$

The Bouguer correction (reduction) is applied in opposite sense to the free air correction, i.e., it is subtracted when the station is above the geoid and vice-versa.

2.4.4 Computation of the Different Gravity Anomalies

Any local deviation of gravity from a more regular or smooth trend, which is defined by a group of several to many stations is an anomaly. Such anomalies are usually the primary data from which a geological interpretation of their source is attempted.

I. Free Air Anomaly: - Only the effect of elevation of a station from the geoid is considered by the free air anomaly. Here the attraction of materials between

the station and the sea level (the geoid) will not be taken into account and that is why it is called the free-air. Thus, this free air anomaly is given by

$$\Delta g_{FA} = g_{obs} + 0.3086h - g_o \quad \text{...(49)}$$

where g_{obs} is the observed gravity, go is the theoretical gravity and h is the elevation.

II. Bouguer Anomaly: -The Bouguer anomaly is the difference between the measured value at the point of observation and the theoretical value calculated for that elevation or water depth, by considering a Bouguer slab of appropriate density for the effect of earth's material between the geoid and the station. The Bouguer anomaly calculated by ignoring topographic effects is known as simple Bouguer anomaly.

$$S.B.A. = gobs + 0.3086h - 0.1119h - go \quad \text{......................(50)}$$

When all corrections, the free-air, Bouguer, together with the terrain correction (δgT) are applied to the observed gravity, the resulting anomaly obtained by subtracting the standard theoretical gravity at the given latitude is called the Complete Bouguer Anomaly (ΔgB) and is given by

$$\triangle gB = gobs + 03086h - 0.1119h + \delta gT - gO \quad \text{......................(51)}$$

2.4.5 Interpretation

The interpretation problem usually is finding the mass distribution for the residual anomaly. Isogal maps look very like topographic contour maps. They show circular, elongated and irregular area of high and low gravity. They may also show linear belts of steep gradients which are not necessarily associated with any of the features just mentioned. It is possible merely from inspection of the map to make a tentative qualitative interpretation if something is known about the geology. Depending on their relief and the distance between axes, this may be interpreted as being indicative of structural features or trends which may be attributed to deformation in sediments or to density contrasts in the basement or both. Gravity highs are in many areas associated with anticlines or with horst blocks, both being structures which bring older, denser rocks nearer the surface. In other regions gravity highs may be due to the presence of

heavy basic intrusions. Conversely sedimentary basins and relatively light acid intrusions usually produce gravity lows. The belts of steep gradients are produced by vertical contacts between rocks of different density such as may occur across fault planes.

If an interpretation is to be quantitative to any degree at all, there must be density information from measurements or more commonly, from inferences based on the general nature of the rocks, which can be learned from existing geological studies or maps of the area, if any. Quantitative interpretation means finding out the position, size, and shape of the gravitating mass through analysis of its potential field. Almost all interpretation of gravity data is by indirect methods. From inspection of the isogal maps taking into consideration all other information about the region, a possible model of the structure is devised and its gravity effect calculated. The observed and calculated anomalies are compared, the model then progressively modified and its anomaly recomputed until a reasonable fit between the two is obtained. If the geological data are scanty it may not be possible to do more than calculate a range of approximate solutions, but even to be able to set limits to the possibilities can be most useful.

When choosing a model it is usual to make the simplest of geometrical approximations as the gravitational attraction of a number of simple forms can be easily calculated from graphs and standard formulae. Since the postulated geometrical shape can at best be only a crude approximation to the real structure, the fit between the calculated and observed anomalies, though often surprisingly good, is unlikely to be 'perfect', i.e. within the limits of observational error, but the procedure does enable an estimate of dimensions and depth to be made quickly. In many instances where there is little geological control there may well be little point in pursuing the interpretation further, since it is highly unlikely that a more complicated model will be a better approximation to the true structure, however exact the fit between the observed an calculated anomalies.

Spheres, cylinders and slabs are the usual geometrical forms chosen when making preliminary interpretation. Since gravimeters respond only to changes in the vertical component of the gravitational anomaly, formulae are required giving the change in the vertical component of the attraction along a traverse at the surface across the body.

Large-scale deep-seated structures predominate on the gravity map to such an extent that it may be very difficult to recognize smaller or shallower features which are the interesting anomalies in gravity survey. The removal of the so called regional resulting from these deep structures is a serious problem in gravity methods. It should be emphasized that, in describing the regional as the effect of 'large-scale deep structures', the latter phrase must be considered in terms of the scale of the survey; the same consideration should apply to the residual(resulting from smaller or shallower features). It would be quite correct to define the regional as the effect in which we are not interested (Telford, 1990).

CHAPTER THREE

3. Data Processing and Presentation

3.1 Gravity Method

The source of the gravity data, employed in this study, is the Geological Survey of Ethiopia (GSE), department of geophysics. The data have already been reduced and processed following the appropriate procedures, including terrain correction, and hence represent the complete Bouguer anomaly. On potential field geophysics, large-scale regional structures pre-dominate gravity and magnetics maps, to an extent that it may be very difficult to recognize smaller or shallower features. Therefore, separation of the regional effect to obtain local features is of paramount importance. In the present study, further processing of the gravity data, including separation of regional and residual components from the Bouguer anomaly, were all performed using a "LINUX" script that involves a series of GMT (Generic Mapping Tool) commands. The regional component is approximated by fitting a lower order polynomial representing a linear trend. The corresponding residual anomalies were then obtained by removing (subtracting) the above mentioned regional trend from the total Bouguer map. The results are presented on figure 4.3.

3.2 Magnetic Method

The end result of a magnetic survey is a contour map of diurnal corrected data. Most of the total field magnetic data is obtained from the work (Tebebe 2006) and is complemented by recent addition, collected by the author.

The data are smoothed by using a moving average filter soft to minimize the effects of outliers arising from personal errors and/or cultural noises. Fig.(4.2c) is a contour map of the total field.

3.2 Electrical Method

50 VES data each of which with maximum pseudodepth (AB/2) of 1000m were obtained from WWDSE. The apparent resistivity values of all the VESs, within the area of interest, are girded and contoured. The results are given as the depth-slice stacked map (figure 4.4) and a vertical, pseudo-depth section, figure 4.8. A contoured map of the lateral variation of apparent resistivities, at a pseudo-depth of 750m is also given as figure 4.5.

A total of 8692 electrical imaging data that covered a distance of about 17.5km along a traverse perpendicular to the inferred barrier were obtained from WWGSE. RES2DINV ver. 3.53 software is used to determine a 2D geoelectric model for the electrical imaging data. Figure (4.6) shows the model.

RES2DINV is a computer program that will automatically determine a 2-dimentional (2-D) resistivity model for the subsurface for the data obtained from electrical imaging surveys (Griffiths and Barker, 1993). The 2-D model used by the inversion program generates a number of rectangular blocks whose arrangement is loosely tied to the distribution of the data points in the pseudo-section. The program automatically decides the number and size of the blocks, using the distribution of the data points as a rough guide. The depth of the bottom row of blocks is set to be approximately equal to the equivalent depth of investigation (Edwards, 1977) of the data points with the largest electrode.

A forward modeling subroutine is used to calculate the apparent resistivity values, and a non-linear least-square optimization technique is used for the inversion routine (deGroot-Hedlin and Constable 1990, Loke and Baker 1996). The program supports both the finite-difference and finite-element forward modeling techniques.

The inversion routine used by the program is based on the smoothness-constrained least-square method (deGroot-Hedlin and Constable 1990, Sasaki 1992). The smoothness-constrained least-square method is based on the following equation

$$\left(J^T J + uF\right)d = J^T g \quad \ldots\ldots\ldots\ldots\ldots\ldots\ldots\ldots\ldots\ldots\ldots\ldots(39)$$

Where $F = f_x f_x^T + f_z f_z^T$

f_x is horizontal flatness filter

f_z is vertical flatness filter

J is matrix of partial derivatives

u is damping factor

d is model perturbation vector

g is discrepancy vector

One advantage is that the damping factor and flatness filters can be adjusted to suit different types of data.

The 2-D model used by this program divides the subsurface into a number of rectangular blocks. The purpose of this program is to determine the resistivity of the rectangular blocks that will produce an apparent resistivity pseudosection that agrees with the actual measurements.

The optimization method basically tries to reduce the diference between the calculated and the measured apparent resistivity values by adjusting the resistivity of the model blocks. A measure of this difference is given by the root-mean-square (RMS) error. However, the model with the lowest possible RMS error can sometimes show large and unrealistic variations in the model resistivity values and might not always be the best model from a geological perspective. In general, the most prudent approach is to choose the model at the iteration after which the RMS error does not change significantly. These usually occur between the third and fifth iterations.

CHAPTER FOUR

4. Results and Interpretations

4.1 Introductory View

Figure 4.1 is presented, in this section, in order to facilitate the discussion of the main findings from the present work by indicating the locations of the different profile lines along which the geophysical surveys have been conducted, with respect to the position of the inferred regional groundwater barrier.

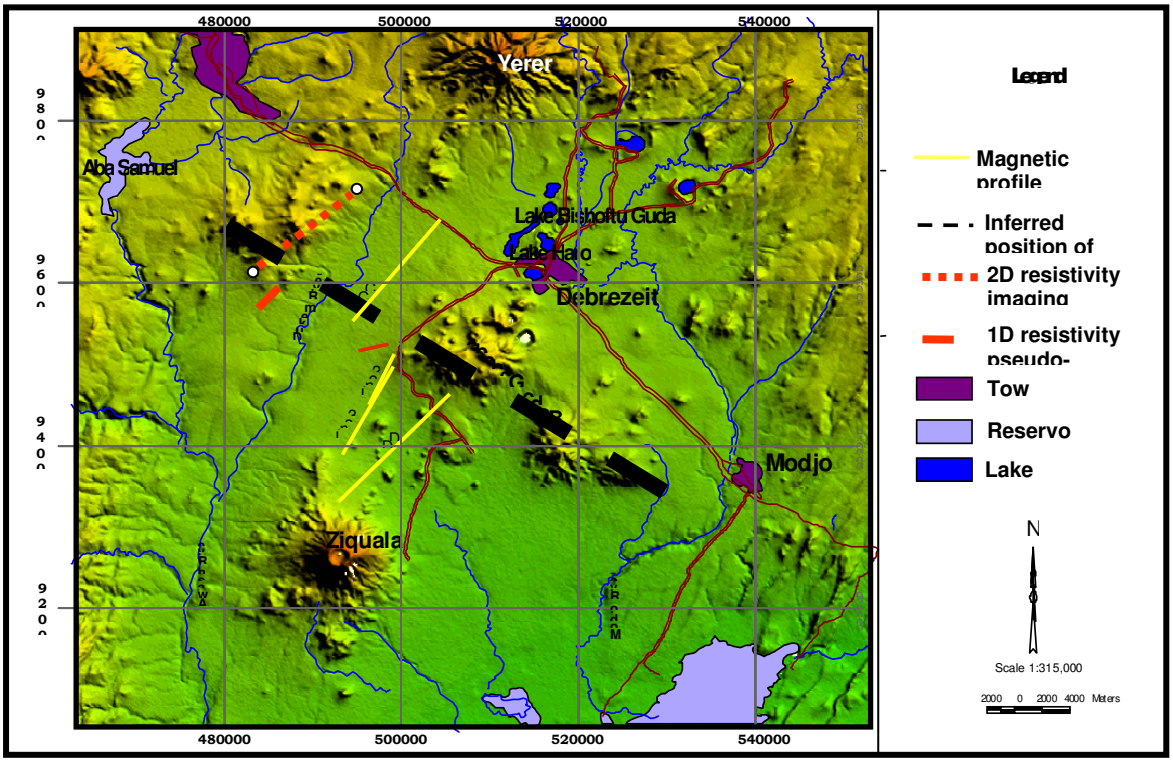

Figure 4.1 Digital topographic model of Ada'a plain and the surrounding area.

Moreover, the digital topographic image clearly shows the major morphological features within the area of interest, and as such, helps to correlate subsurface geophysical signatures with their respective surface manifestation.

Figure 4.2, subsequently, gives a perspective view regarding the relative proportion of the area coverage of the different geophysical methods.

Figure 4.2(a) shows the regional Bouguer gravity map of central Ethiopia flanking the western margin of the Main Ethiopian rift.

The regional Bouguer anomaly map is used, in this study, as a general guideline by indicating the overall orientations of the major structural features and outlining the trends of smaller scale local bodies within the area of interest and its immediate surrounding regions.

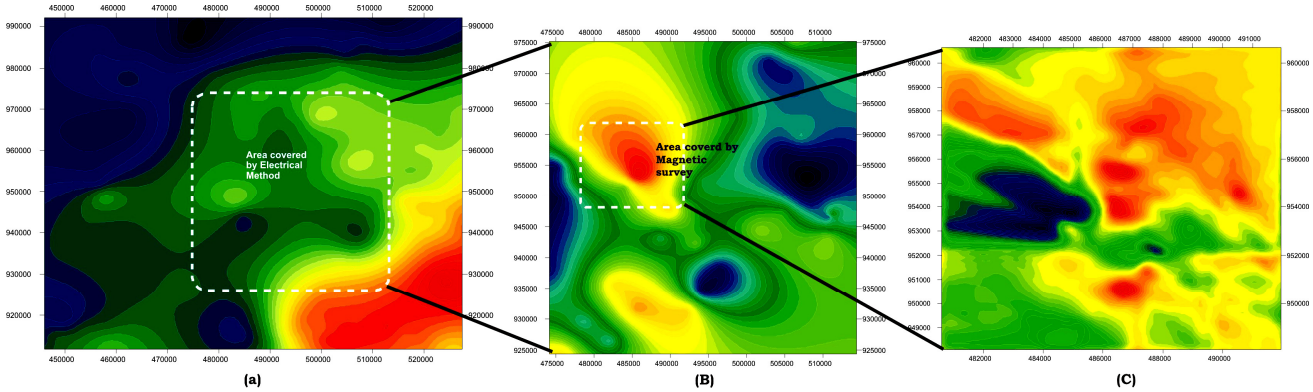

Figure 4.2 Regional Bouguer anomaly map (a), apparent resistivity plan map at slice depth of 750m (b) and total field magnetic field map (c).

Accordingly, the extreme high and low gravity responses that occupy the NW and SE corners of the Bouguer gravity map suggests that the dominant regional structures have a general NE-SW orientation and possibly related to the main Ethiopian rift.

In the intermediate response regions, which also display a similar trend, there are some local features, medium amplitude anomalies, with different alignment to that of the regional trend, i.e., in the NW-SE direction.

The Vertical Electrical Soundings, carried out by the Enterprise, some of which are used in this dissertation work, covers relatively smaller area and are largely concentrated within the central region covered by the gravity map. For the purpose of correlation and comparison, the region coved by electrical survey is indicated by the white box on figure 4.2 (a).
The lateral variation of apparent resistivities at a pseudo depth (ab/2) of 750 m is shown on figure 4.2 (b). A strong, high resistivity anomaly, apparently elongated in the NE-SW direction (as indicated by the local Bouguer anomalies), is the dominant feature of the map.

Finally, the total field magnetic map, comprising data collected by the author and (Tibebe, 2006), is presented in figure 4.2 (c) and covers a good part of the high resistivity anomaly shown on figure 4.2 (b). The general magnetic response of the area is also indicative of NE-SW orientation of the causative bodies, in agreement to the results of the regional gravity and electrical resistivity surveys.

The preliminary analysis made on the main features of these three independent regional geophysical surveys strengthens the speculation on the existence of a subsurface structure oriented in a NW-SE direction and is spatially tally to the Bede-Gebaba ridge.

To examine the existence of this anticipated barrier, acting as a ground water divide separating two ground water regimes, NE and SW of the Bede-Gebaba ridge, is the principal objective of this study. The subsequent sections, therefore, discuss the results of the geophysical data analysis in detail.

4.2 Regional Bouguer Gravity

Referring to the left hand plate of figure 4.3, the Bouguer anomaly map generally exhibit two contrasting zones, separated by a NE to SW running intermediate amplitude response region. The north-west area is dominated by relatively lower Bouguer values while the area south-east of the divide generally shows relatively higher Bouguer responses. The highest amplitude anomaly values (-160 mGal) is observed in the south-eastern zone and is thought to arise from western margin of the main rift. Moreover, northwestern part is dominated by lower values (-220 - -210mGal) and coincides with elevated land mass. The intermediate Bouguer values, ranging between -195 to -185mGal, occupy the region between the contrasting regions. The area around Debre-Zeyt and Ada'a plain are all included in this intermediate Bouguer zone and is reflective of its geology which is mainly covered by acidic to intermediate volcanic and sedimentary rocks.

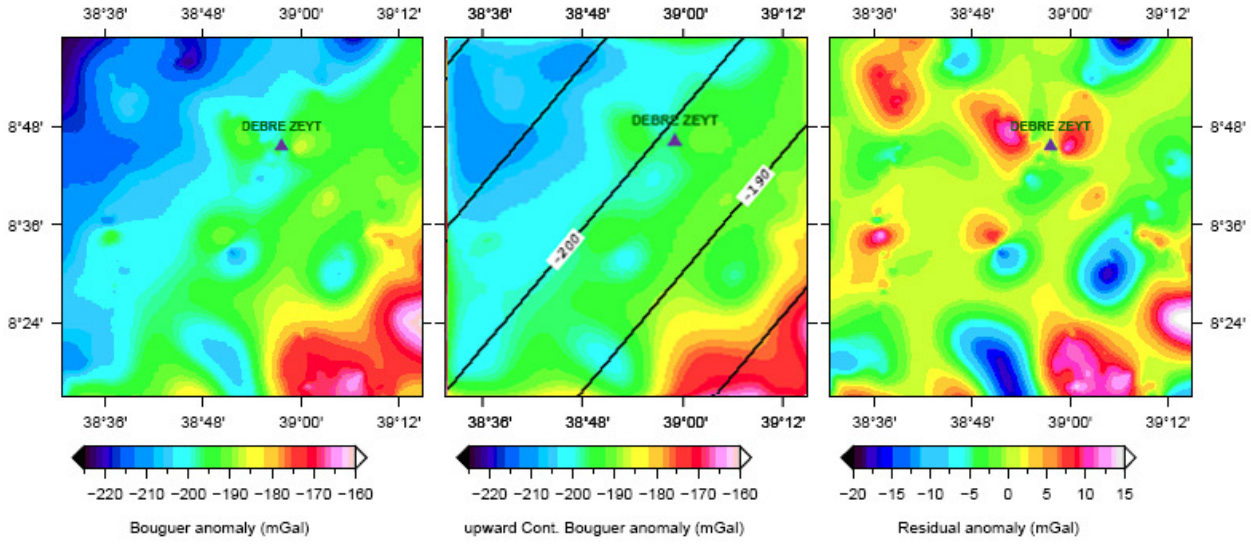

Figure 4.3 Total Bouguer (left), linear regional trend superimposed on upward continued (center) and residual Bouguer map (Right).

The regional component of the Bouguer anomaly is presented as a contour trend superimposed on the map of upward-continued values to a height of 1.5km, the middle plate of Fig (4.3). The regional variations that have long wavelength and low amplitude are perceptible over large distances and are thought to be generated by broad crustal structures at relatively deep-seated bodies. Like the total Bouguer map, the regional structural trend follows a NE-SW direction and is indicative of the dominance of the main Ethiopian rift, specially its western escarpment.

The residual Bouguer anomaly map, (the right hand plate of figure 4.3, shows the value varies from a minimum of -20 to a maximum of +15mGal. The residual anomaly map shows a number of distinct features than that of the Bouguer anomaly map indicating that the effect of the local anomalies were masked by the regional effect.

Volcanic activity in the area has given rise to central composite volcanoes as well as to monogenic apparatea as domes, spatter cones and maars. Ignimbrites, consisting of several units, appear as wide sub-horizontal covers, while basaltic lavas are generally tabular. The residual Bouguer map, therefore, reflect the geologic reality of the region where the localized anomalous patches represent the domes and cones of intermediate lava formed by volcanic activities while, the vast background response reflect the vast acidic to intermediate volcanic and sedimentary rocks.

The most interesting feature, in the context of the main objective, is that of the strong positive residual anomaly, west of Debre-zeyit town. Elongated in NW – SE direction, it represent the intermediate amplitude patches that appear in the total Bouguer map oriented in opposite direction to the regional trend. The position and orientation of this particular anomaly closely matches to that of the Bede-Gebaba ridges.
The spatial correlation of the inferred subsurface barrier, which is also believed to have a similar NW – SE trend along the extension of the Bede-

Gebaba ridge, to the residual Bouguer anomaly may be considered as additional evidence to accredit its existence.

4.3 Magnetic survey

A large amount of the effort put into interpreting magnetic data obtained in magnetic exploration goes no farther than a qualitative evaluation of magnetic maps. The processed magnetic data discussed in section 3.2 resulted in the contour map in figure 4.1(c). These data dominated over the area enclosed by the white box in figure 4.1(b) that is right at the speculated barrier. The high relief and the steep gradient observed in the magnetic contours elongated NE to SW represent domes and cones of intermediate lava formed by volcanic activities. The smooth contours and low magnetic relief, SW of the magnetic contour map, SW of the map, may be extension of the vast background low apparent resistivity response that reflect the vast acidic to intermediate volcanic and sedimentary rocks.

4.4 Electrical Resistivity Survey

Figure 4.4 shows depth-slice stack of apparent resistivity contour maps at pseudo depths (AB/2) of 4.2m, 100m, 220m, 500m, 750m and 1000m.
At shallow depth, the ground is electrically homogenous and conductive. Zoning of the ground comes to picture at deeper horizons and is marked by sharp apparent resistivity contrasts. The vast high resistivity (> 250 Ohm-m) zone, visible on south and south-eastern portion of the survey area, shows comparable amplitude and apparently occupies similar position on slice maps of 100m and 200m pseudo-depths. The narrow elongated, resistive (~ 200 Ohm-m) patch, in the upper central region, however, seems to broaden at the lower level. On the pseudo-depth of 750 m, this anomalous zone extends both ways, apparently elongated in the NE-SW direction.

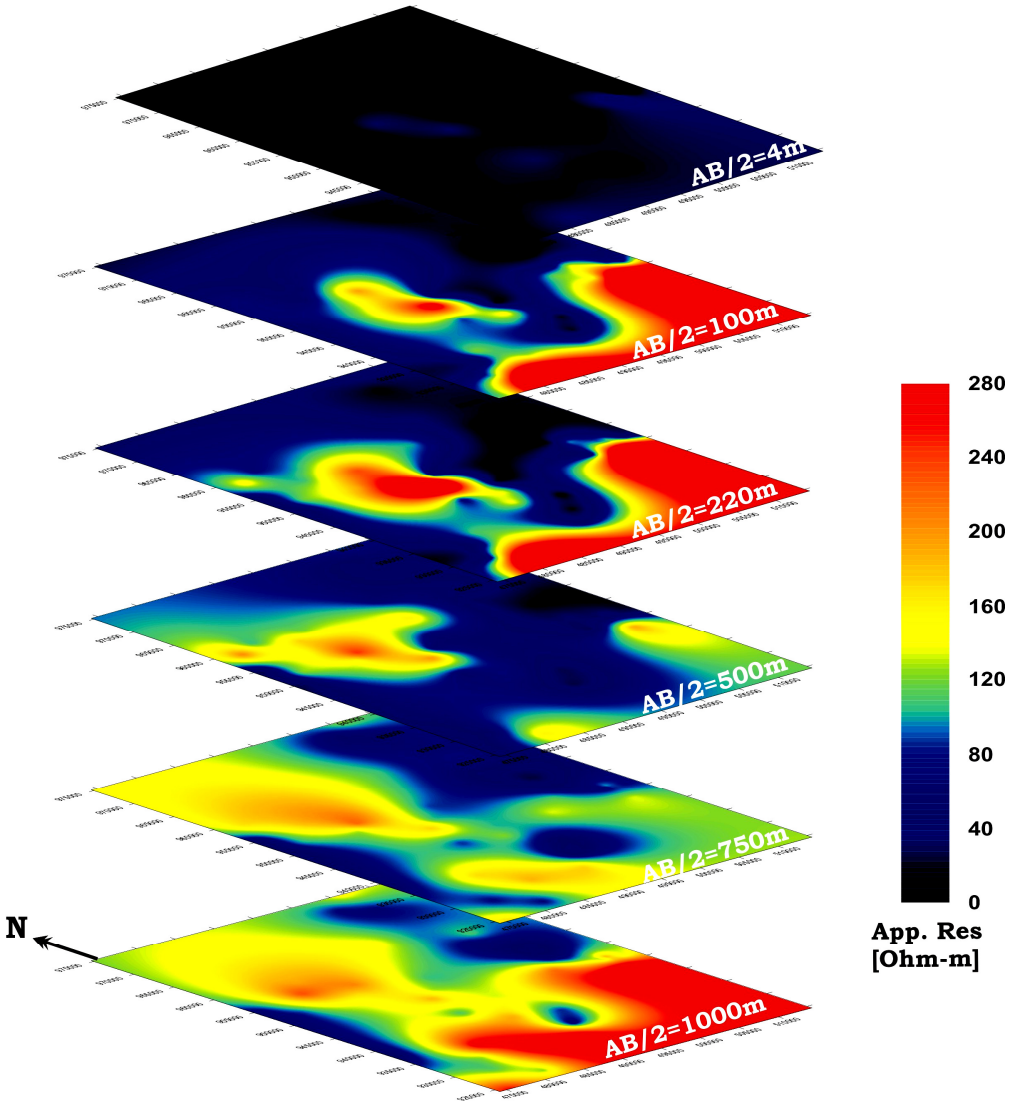

Figure 4.4 Stacked apparent resistivity sections at various depth levels

On either side to this elongated high resistivity feature, there happen to be conductive horizons, which are quite unusual for such depth level. The

bottom level map, at ab/2=1000m, indicates that the two conductive horizon continues downward with depth, separated by the elongated resistive body.

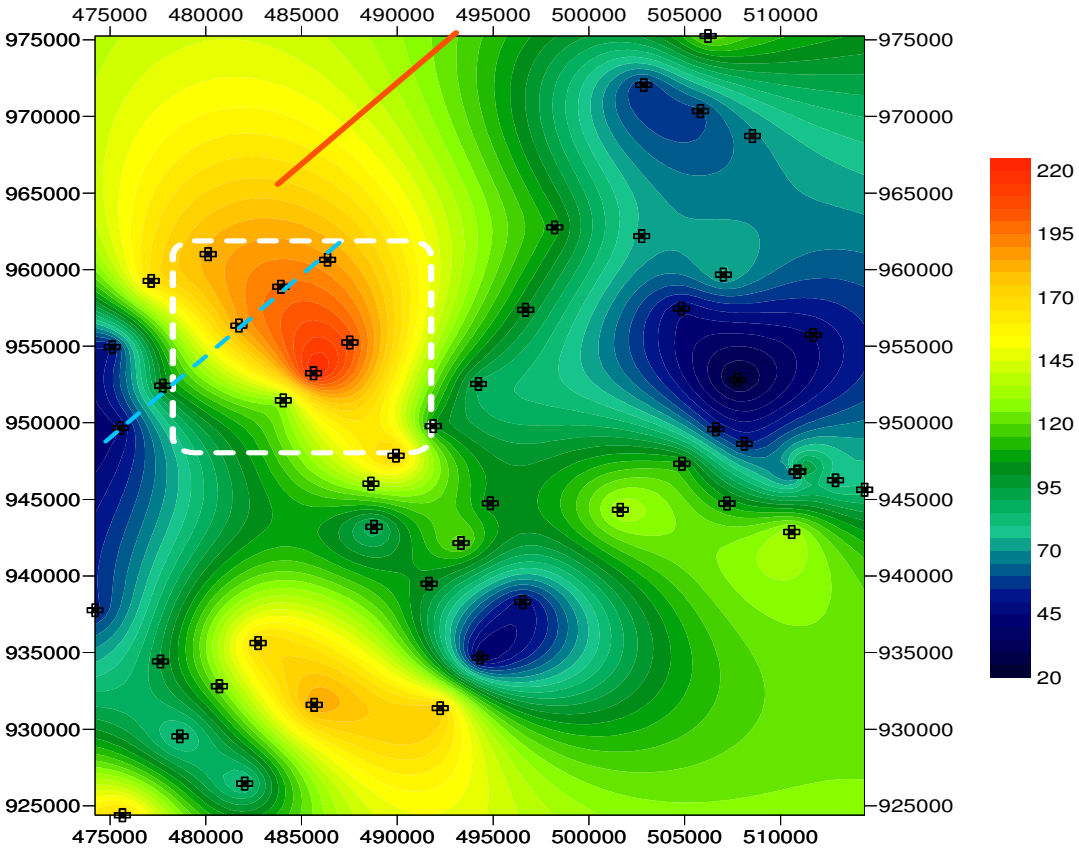

Figure 4.5 Lateral apparent resistivity section at ab/2=750m, showing the positions of the sounding points, the 2D image profile and 1 1D apparent resistivity pseudo-section.

Figure 4.5, depicts the lateral variation of apparent resistivity at ab/2=750m, and will be discussed in further detail to highlight the geoelectric nature of the subsurface and its hydro-geological significance. Moreover, the figure illustrates the spatial correlation between the other two depth sections by showing the positions of the sounding points, the 2D resistivity imaging profile-line and the position of the 1D apparent resistivity pseudo-section.

The aquifers of Ada'a plain are lacustrine sediments, scoria, scoraceous basalt and vesicular basalts (volcanic aquifers). The thickness of lacustrine sediments can reach up to 100 m, underlain by scoraceous basalt. Hence the

homogenous conductive upper horizon is the likely response of the Lacustrine and Alluvial sediments, dominant within the top few tens of meters of depth. Owing to the inherent interstitial space and electrically conductive components, like clay, these sediments generally offer low resistivity for the passage of electric current, as compared to crystalline rocks.

Volcanic rocks, on the other hand, are known to be electrically resistive unless posse substantial amount of fluid in the interconnected internal space. In the volcanic ground, water circulation and occurrence (storage) is associated with primary porosities like vesicles, and secondary porosities like faults, fractures and fissures produced as a result of tectonic activities and weathering.

The two conductive zones, which have been shown to extend down to a considerable depth probably reaching the volcanic section of the subsurface, could safely be attributed to water saturated, aquifer zones. The resistive portion that divides the two likely water-bearing horizons may represent a dry impermeable rock unit.

In the following section the results of the 2D resistivity imaging on the inferred barrier, and 1D depth pseudo-section are discussed.
Figure 4.6(a) shows pseudo-section of the measured apparent resistivity data of the 2D resistivity imaging carried out along the profile-line illustrated in figure 4.5.

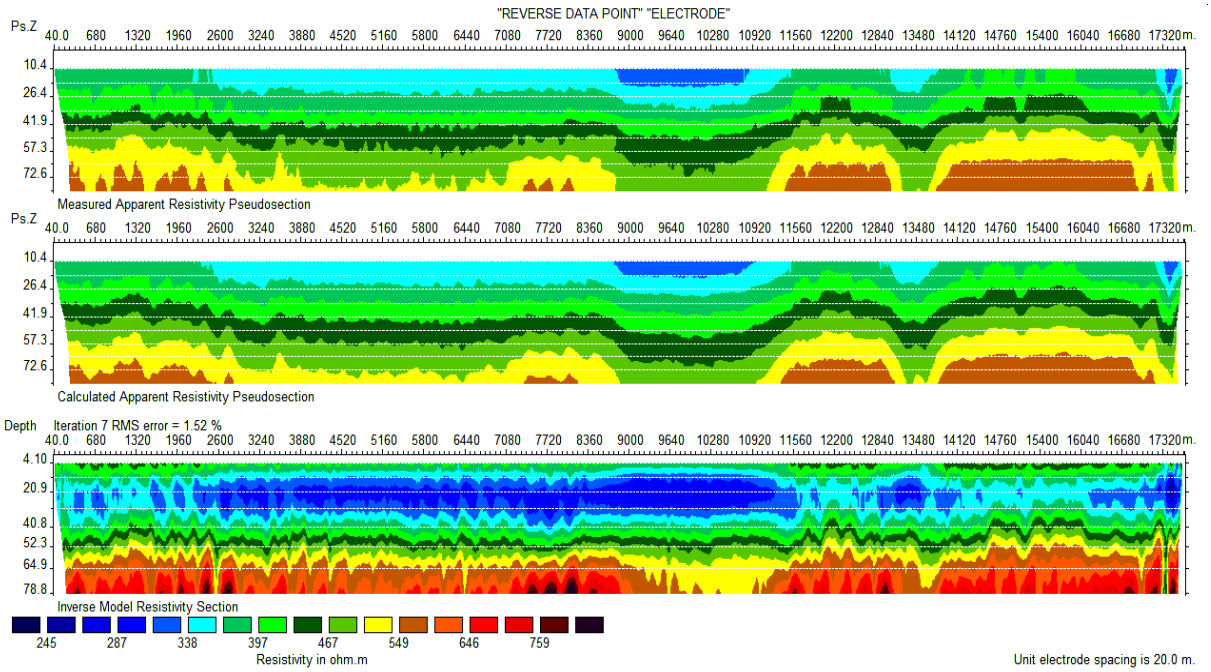

Figure 4.6 2D Electrical imaging (upper) measured apparent resistivity pseudo-section, (middle) calculated apparent resistivity pseudo-section and (bottom) geoelectric model.

A geo-electric model of the subsurface along the described profile-line was developed using a 2D electrical resistivity imaging inversion software and the result is given in figure 4.6(bottom). The program develops the model by calculating the true resistivity values of the ground section, from the measured apparent resistivity. Figure 4.6(middle) shows the theoretical model, calculated apparent resistivity section. The striking resemblance between the upper, measured apparent resistivity section 4.6(upper) and the middle calculated response 4.6 (middle), is indicative of the model reliability.
The model depicts a wide range of resistivity and is characterized by progressively increasing formation resistivity with depth. Though the resistivity response appears somehow high for shallow portion of the subsurface, the lateral variation at deeper horizons reflects the morphology of the resistive bottom.

Referring to figure 4.6(middle), the resistive substratum, which may act as aqua-clued appears to rise to the surface towards the right end of the profile,

starting from the 11th km. Consequently, the 30 - 40m deep water table, as discovered from a borehole data obtained from WWDSE, lies below the top of this resistive and possibly impermeable subsurface feature which is shown to rise as shallow as 43m. The resistivity imaging survey, nevertheless, failed short to show the right hand boarder of the body. Based on the available image and taking the results of the other geophysical methods, it may still be safe to correlate the resistive body to the inferred barrier. Further more as this high resistivity response may be due to volcanic intrusion, this could possibly impede the ground water movement.

As it is shown on figure 4.5, the projection of the 2D resistivity survey line on the depth slice plane section, it ends before transecting the resistive horizon, which is also attributed to the inferred barrier. Hence, it is worth to consider the VES data close to the area of interest for additional information.
A vertical resistivity pseudo depth section, shown in figure 4.7, is constructed along a line joining five VES points namely, 54,55,56,57 and 59. This is thought to complement the electrical imaging since it gives a contrast from the opposite end.

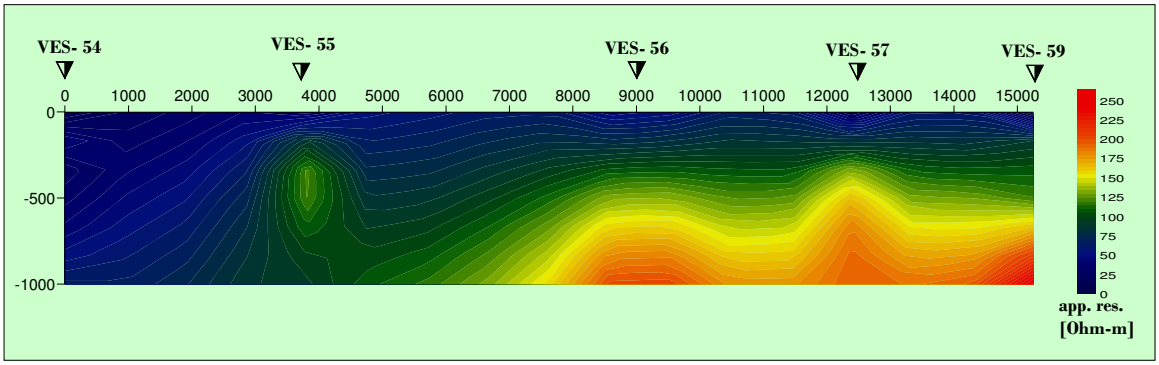

Figure 4.7 a resistivity pseudo-section along a line connecting VES-54, -55, -56, -57 and 59.

Accordingly, the right flank of the depth section reveals that high resistive signature of the anticipated barrier extends further, for about 6 km, before plunging down between VES-55 and -56.

CHAPTER FIVE

5 Conclusions and recommendations

5.1 Conclusions

An over all view of the results of the study has led to the following summarized conclusion.

The residual Bougeur anomaly contour map has revealed small scale, local subsurface structure with discordant structural alignment that has spatial correlation with the expected subsurface barrier. The depth-slice stack map of apparent resistivity of fifty VES data has also manifested this body as a high resistivity structure that separate two conductive zones, which have been shown to extend down to a considerable depth, probably reaching the volcanic section of the subsurface that could safely be attributed to water saturated, aquifer zones.

This feature may be interpreted as an impermeable dry rock units related to domes and cones of intermediate magma that can possibly impede the ground water movement. The 2D electrical imaging and the 1D apparent resistivity pseudo-section reflect this geologic reality. It is, thus, likely that the inferred ground water barrier exists.

The application of the integrated geophysical method has facilitated the data interpretation and has greatly reduced the ambiguity inherent in each method.

The results of the different geophysical methods have shown good correlation with each other, highlighting the merits of the use of integrated geophysical survey.

5.2 Recommendations

1. Two conductive zones, which have been shown to extend down to a considerable depth, probably reaching the volcanic section of the subsurface could safely be attributed to water saturated, aquifer zones are recommended to be followed up as a potential of ground water.

2. The 2D resistivity survey line ends before transecting the resistive horizon. The survey failed short to show the right hand boarder of the body, which is also attributed to the inferred barrier. Extension of the traverse to the right hand border is recomended in order the imaging survey to be complete.

3. Adequate coverage of the plain by gravity and magnetics data can provide additional information on the area and as such facilitate complete understanding for further planning.

4. None of the traverse lines presently fully cross the inferred barrier. VES, magnetic, gravity and electrical resistivity profiling data along parallel traverses perpendicular to the inferred barrier are recommended to verify the existance of the inferred barrier more reliably.

List of References

[1] Breiner, S., 1973: "Applications Manual for Portable Magnetometers," Geometrics, California.

[2] Burger H.R., 1992. Exploration Geophysics of the shallow subsurface, Prentice-Hall, Inc. New Jercy.

[3] deGroot-Hedline, C. and Constable, S., 1990, Occam's inversion to generate smooth, two-dimentional models from magnetotelluric data. Geophysics.

[4] Edwards, L.S., 1977. A Modified Pseudosection for Resistivity and Induced Polarization.

[5] Dobrine, M.B., 1976. "Introduction to Geophysical Prospecting," McGraw-Hill Company, USA.

[6] Dobrine, M.B., and C.H. Savit , 1988. "Introduction to Geophysical Prospecting," McGraw-Hill Company, New York.

[7] F. Mazzarini, 1999. Journal of the National Volcanic Group of Italy, vollum II.

[8] Gerkens, T.C.,1989. "Foundation of Exploration Geophysics" Elsevier Scientific Publishing Company, Amsterdam.

[9] Griffiths D.H and Baker R.D. 1993, Two-dimensional resistivity imaging and modeling in areas of complex geology. Journal of Applied Geophysics.

[10] Halcrow, 1989. Master Plan for the development of surface water resources in the Awash basin, Volume 5.

[11] Inception Report, 2006. Evaluation of Water Resources of the Ada'a Plain Ground Water Basin for Irrigation Development Project. Federal Democratic Republic of Ethiopia Ministry of Water Resources.

[12] Keller, G.V., and F.C. Frisehknecht, 1966. "Electrical methods in Geophysical Prospecting," Pergamon press, Oxford.

[13] Loke, M.H. and Barker, R.D., 1996a, Rapid least-squares inversion of apparent resistivity pseudosections by a quasi-Newton method. Geophysical prospecting.

[14] Mohar, P.A., 1971. The Geology of Ethiopia University College of Addis Ababa Press.

[15] Nettleton, L.L., 1976. "Gravity and Magnetics in Oil Prospecting," McGraw-Hill Book Company, New York.

[16] Parasnis, D.S., 1975. "Mining Geophysics," Elsevier Scientific Publishing Company, Amsterdam.

[17] Parasnis, D.S., 1979. "Principles of Applied Geophysics," CHAPMAN HALL, London.

[18] Parasnis, D.S.,1986. "Mining Geophysics," Elsevier Scientific Publishing Company, Amsterdam.

[19] RES2DINV. 2003, Geoelectrical Imaging 2D and 3D, Geotomo Software.

[20] Reynolds, 1997. "Introduction to Applied and Environmental Geophysics," John Wiley and Sons Ltd. England.

[21] Sasaki, Y., 1992, Resolution of resistivity tomography inferred from numerical simulation. Geophysical prospecting.

[22] Telford, W.M., L.P. Geldart, R.E. Sheriff and D.A. keys, 1976. "Applied Geophysics," Cambridge University Press, London.

[23] Telford, W.M., L.P. Geldart, R.E. Sheriff and D.A. keys , 1990. "Applied Geophysics, 2nd edn." Cambridge University Press, London.

[24] Tesfaye Chernet, 1986. Hydrogeology of Ethiopia.

[25] Tibebe, 2006. Application of Electrical Resistivity and Magnetic Methods for the Evaluation of Ground Water at Ada'a Plain. A Thesis Presented to the School of Graduates of Addis Ababa University.

[26] Torge, W., 1989. Gravimetry, Walter de Gruyter & Co., Berlin, Germany.

[27] Van Nostrand R., and Cook G., 1966. Interpretation of Resistivity Data. United States Geological Survey Professional Paper, Vol. 499.

[28] Zohdy, A.A.R. 1974. "Electrical Methods in: Applications of Surface Geophysics," USGPO.

DECLARATION

I, the undersigned, hereby declare that this thesis is my original work and has not been presented for a degree in any other University, and all sources of material used fro the thesis have been duly acknowledged.

Name: Assefa Getaneh

Signature: _____

This thesis has been submitted for examination with my approval as University advisor.

Name: Dr. Shemels Fisseha

Signature: _____

Date: _____